[American Journal of Science, Vol. 305, May, 2005, P. 369–406]

ASYMMETRIC GROWTH OF THE PYRENEES REVEALED THROUGH MEASUREMENT AND MODELING OF OROGENIC FLUXES

H. D. SINCLAIR*, M. GIBSON*, M. NAYLOR*, and R. G. MORRIS**

ABSTRACT. Orogenic asymmetry is ubiquitous in terms of topography, structure and metamorphism, but the relative influences of climate and tectonics in determining such asymmetry remain contentious. This study demonstrates that for the case of the European Pyrenees, orogenic asymmetry is not defined by inherited structural asymmetry, nor by orographic asymmetry of precipitation, but is the simple consequence of the inherent tectonic growth of a doubly-vergent orogen.

The Pyrenees record approximately 60 Myr of upper crustal accretion, erosion and sedimentation that developed from Late Cretaceous to early Miocene times. Approximately 165 km of plate convergence was accommodated by four phases of orogenic growth that can be summarized in terms of their generic orogenic development as follows: 1) Early inversion of passive margin extensional faults, initiating the pro-wedge. 2) Growth by a combination of frontal accretion and underplating to the pro-wedge; symmetrical and steady record of erosion and foreland basin sedimentation. 3) Cessation of pro-wedge frontal accretion with propagation of the retro-wedge deformation front. 4) Accelerated growth of pro-wedge antiformal stack induced by underplating; accelerated erosion over antiformal stack and increase in sediment discharge to pro-foreland basin; stabilization of outer pro-wedge by sediment blanketing.

Discrete element model experiments are used to explore the natural tendency of the system towards asymmetry. Model output demonstrates that during active frontal accretion to the pro-wedge of an orogen, the maxima in erosional denudation is offset towards the pro-wedge relative to the maximum depths of exhumation. This asymmetry is fundamentally driven by the progressive reduction in advection velocities of material within the orogen from the pro-wedge into the retro-wedge. Hence, for an efficient erosional regime, a dynamic coupling between erosion and structural uplift of the pro-wedge will reduce activity of the retro-wedge and hence drive asymmetry in terms of low temperature thermochronometry, erosion and sedimentation. The models also demonstrate the tendency for pro-wedge growth through frontal accretion to slow. However, the cessation of frontal accretion as recorded by the South Pyrenean Thrust Belt (phases 3 and 4) requires additional forcing; it is proposed that the thick wedge-top sedimentation recorded at this time, increased taper angles and hence stabilized the wedge. Accretionary influx into the orogen at this time was accomplished through underplating. These processes governing asymmetry do not require a spatially variable climate or a laterally heterogeneous underthrust plate.

INTRODUCTION

Significant advances have been made in establishing the potential contributions of climate and tectonics in defining the long-term (10^6 – 10^7 yrs) mechanical and topographic asymmetry in the growth of mountain belts (for example Beaumont and others, 1992; Koons, 1995; Willett, 1999; Burbank and others, 2003). Numerical models have been used to demonstrate that in the absence of erosion, trajectory paths for a parcel of rock accreted from the underthrust plate will be directed towards and over the overthrust plate resulting in a highly asymmetric form. These trajectories through an orogen are significantly deflected when erosion, whether localized or widespread drives the surficial removal of mass. Through this understanding, we now recognize that trajectory paths determine the structural and thermal evolution of the

*School of GeoSciences, The University of Edinburgh, Grant Institute, Kings Buildings, West Mains Road, Edinburgh, EH9 3JW, United Kingdom; hugh.sinclair@glg.ed.ac.uk
**School of Earth Sciences, The University of Birmingham, Edgbaston, Birmingham, United Kingdom

orogen, and so, erosion is now understood as a first-order control on orogenesis (for example Beaumont and others, 1992; Pinter and Brandon, 1997).

Many of the young active mountain belts of the world have been used as the laboratories in which to investigate the natural tectonic forcing of orogenesis, and the potential role played by climatic forcing. Examples include the Southern Alps, New Zealand (Koons, 1990; Norris and others, 1990; Beaumont and others, 1996), Taiwan (Suppe, 1981; Deffontaines and others, 1994), the Olympic Mountains, Washington State (Brandon and others, 1998; Pazzaglia and Brandon, 2001) and the Andes (Montgomery and others, 2002; Lamb and Davis, 2003). In addition, mountain belts that are now relatively inactive contain records of orogenesis from initiation to late-stage decay, and have the potential to record complete histories of mountain building through analysis of multiple geo- and thermochronometers, structural studies and the stratigraphic records of the exposed foreland basins. The European Alps represent an example of such a long-term integrated understanding (Sinclair and Allen, 1992; Schlunegger and Willett, 1999; Pfiffner and others, 2000; Cederbom and others, 2004).

Both numerical and analogue models have been successful in exploring the potential controls on orogenesis. Sand-box experiments have demonstrated the controls on taper angles, and the mechanics of frontal accretion and internal thickening (for example Storti and McClay, 1995). On the scale of entire orogens, finite element continuum models have revealed the importance of horizontal advection of mass through the orogen in determining the asymmetric topographic form of a mountain belt (Willett and others, 2001). In addition, these same models have explored the potential role of orographic precipitation in generating variable erosion that drives trajectory paths (Beaumont and others, 1992; Willett, 1999). They have also enabled quantitative predictions of cooling paths, and hence thermochronometric age distributions across orogens (Batt and others, 2001) that have been used to assess the flux balance in these systems (Willett and Brandon, 2002).

Here, we provide documentation of the long-term (approximately 60 Myr) evolution of the Pyrenees of western Europe in order to quantify the accretionary, erosional and sedimentary flux of the system, and evaluate the underlying controls on its asymmetry. We differentiate the first-order, simple tectonic development of the system from components that we believe require some degree of external forcing (for example additional climatic or tectonic components). This is aided by the use of a series of experiments run using a discrete element model (Burbidge and Braun, 2002; Naylor and others, 2005). The results demonstrate the natural tendency for small, doubly-vergent orogens to focus deformation and erosional unroofing towards the pro-wedge (that portion overlying the underthrust plate) when coupled to an efficient, spatially invariant erosional system. In the Pyrenees, this is achieved through underplating which represents the primary accretionary flux, and which couples directly to the maximum erosional efflux and goes on to determine the asymmetry of sedimentation rates in the neighboring foreland basins. The results revise aspects of current theories of the controls on Pyrenean orogenesis (for example, Fitzgerald and others, 1999; Beaumont and others, 2000) and provide insight into the general interactions between frontal accretion, underplating and erosion during orogenesis.

The data is presented in three components: (1) The thermochronometric data yielding insight into rates and timing of exhumation. (2) The timing of thrust activity based on the history of wedge-top sedimentation; this reveals the rates and timing of frontal accretion to both the pro- and retro-wedges. (3) The sediment volumes and hence sedimentation rates in the two foreland basins (Ebro and Aquitaine basins). These data are then integrated into a flux-based evolutionary model for the Pyrenees,

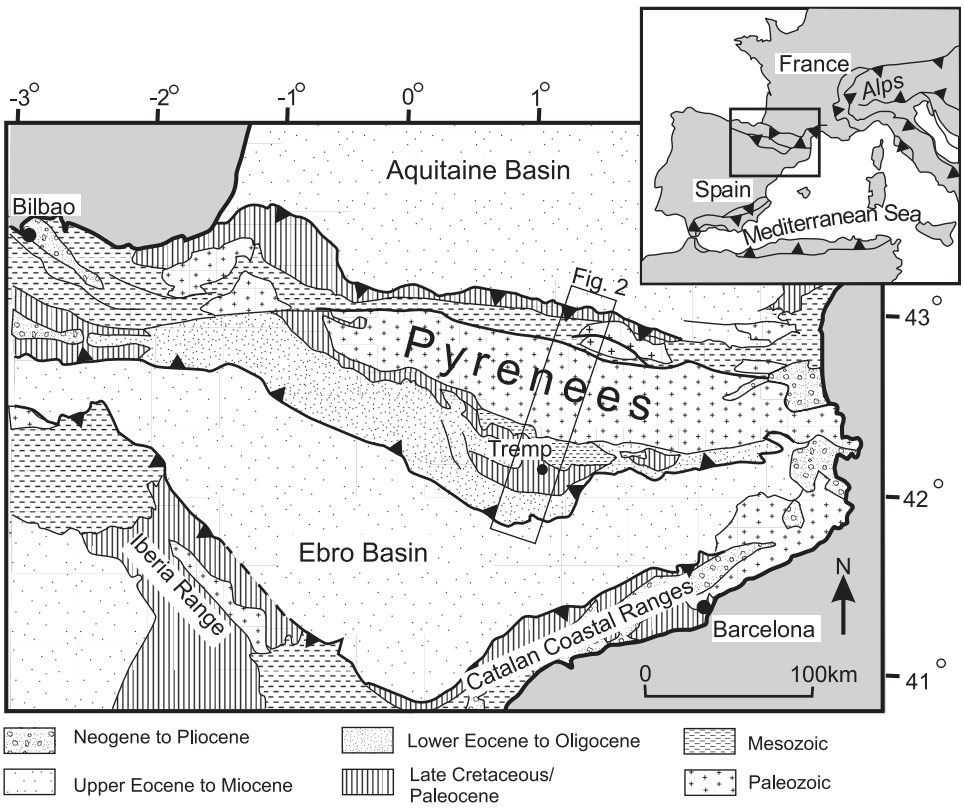

Fig. 1. Geological map of the Pyrenean region of Spain and France. Transect of study is outlined by box.

which is used as the basis for a comparison with predictions from the numerical model experiments.

GEOLOGY OF THE PYRENEES

The Pyrenees formed by the convergence of the Iberian and European plates during Late Cretaceous to early Miocene times (Roest and Srivastava, 1991), involving at least 165 km of shortening and upper crustal thickening (Muñoz, 1992; Beaumont and others, 2000). The ECORS deep seismic reflection profile (Choukroune and others, 1989) in combination with other geophysical data (Pous and others, 1995) indicate that the Iberian plate has been subducted northwards to a minimum depth of approximately 80 km. The surface expression of this collision is a doubly-vergent orogen that is approximately 150 km wide with a central zone dominated by Hercynian basement flanked by thin-skinned fold and thrust belts and associated foreland basins (figs. 1, 2 and 3). The central Axial Zone is separated from the North Pyrenean Zone by the North Pyrenean Fault, which is believed to represent the suture between the material accreted from the European craton versus the Iberian craton (Fischer, 1984). Lying between the North Pyrenean Zone and the Aquitaine Basin are the Sub-Pyrenees which represent a narrow zone of thin-skinned accretion of Tertiary foreland basin strata and are bound to the north by the Sub-Pyrenean thrust front (Deramond and others, 1993).

The Axial Zone and North Pyrenean zones contain numerous igneous and high-grade metamorphic crystalline basement rocks that yield minerals suitable for

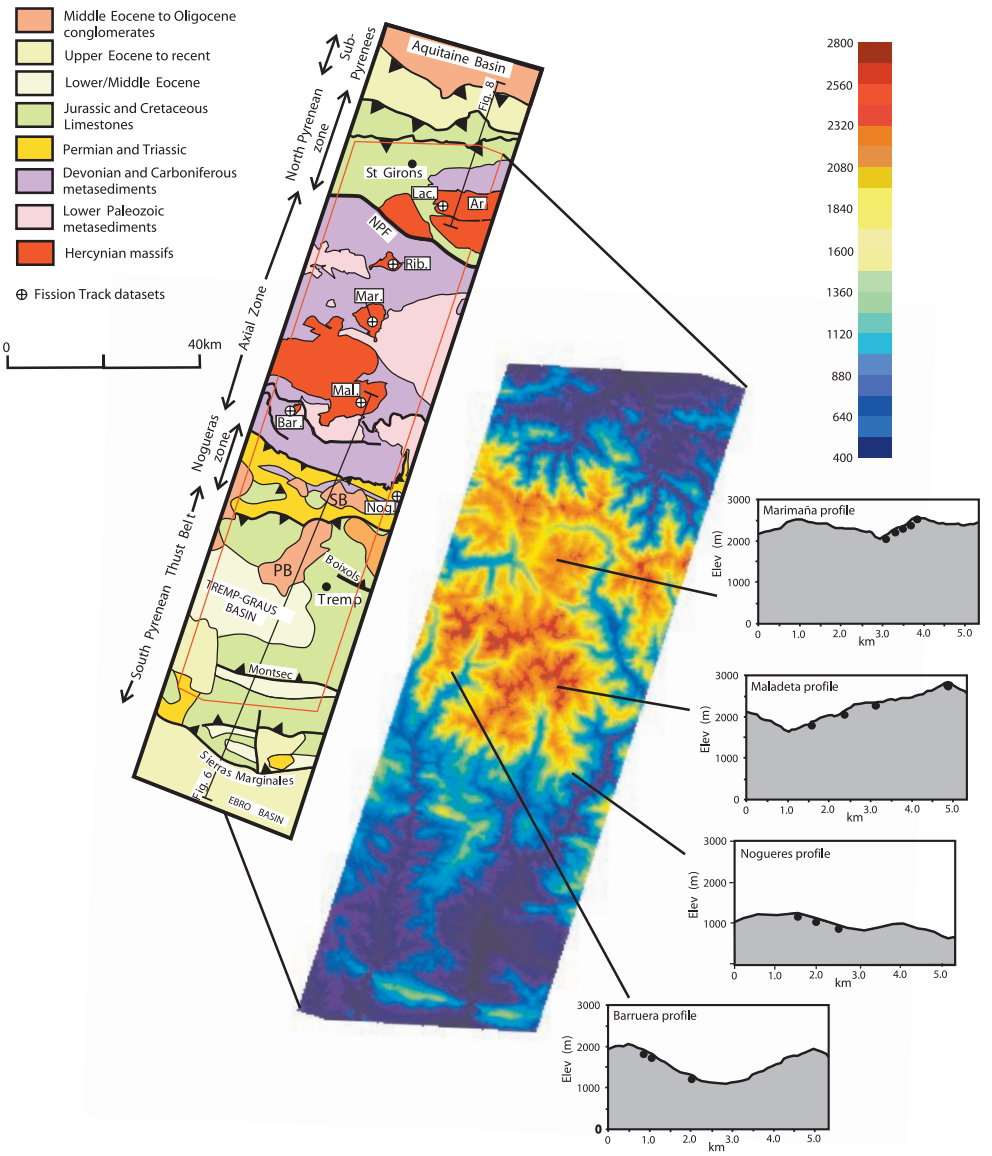

Fig. 2. Geological map across a traverse of the central Pyrenees showing the main structural and lithological units with locations for thermochronological studies. Digital topography across the Axial Zone of the Pyrenees showing sample sites, with topographic details identifying the sampling sites with respect to topography.

thermochronological analyses. Hence, a number of studies have used both individual elevation sampling procedures (Garwin, ms, 1985; Yelland, 1990; Morris and others, 1998) and vertical sampling in order to investigate long-term cooling histories in the orogen (Fitzgerald and others, 1999). The results of these studies have demonstrated the asymmetric exhumation history of the orogen, with greater, and younger exhumation occurring in the south (pro-side) of the orogen. This asymmetry has been simulated using crustal heterogeneities in the underthrust plate as input into finite

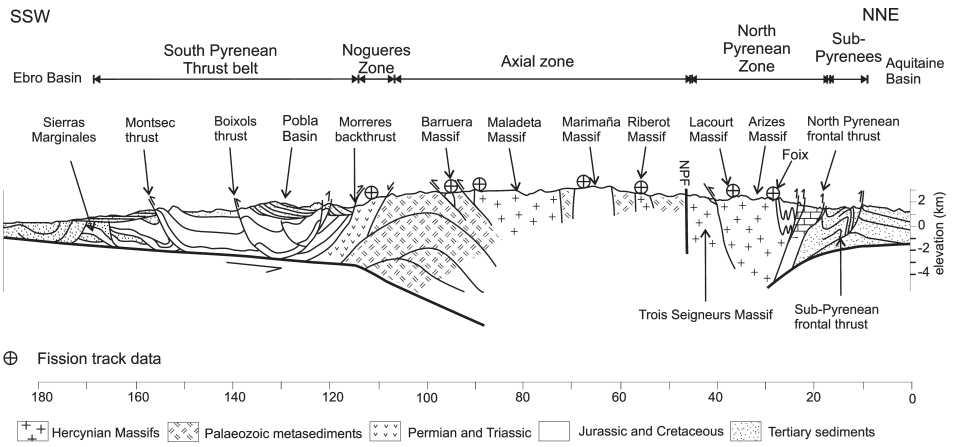

Fig. 3. Structural cross-section following the traverse shown in figure 2 compiled from geological maps (BRGM 1973) and the published literature (Muñoz, 1992; Meigs and Burbank, 1997; Vergés, 1999).

element models; these heterogeneities are interpreted to have enhanced underplating and resulted in the formation of the Axial Zone antiformal stack in the rear of the pro-wedge (Beaumont and others, 2000).

The South Pyrenean Fold and Thrust Belt (figs. 2 and 3) comprises a deformed Mesozoic succession detached on Triassic evaporites and overlain by syn-deformational Tertiary sediments that have been used extensively for documenting the history of thrust motions (for example, Mutti and Sgavetti, 1987; Deramond and others, 1993; Mellere, 1993; Meigs and Burbank, 1997; Williams and others, 1998; Vergés, 1999; see below). The South Pyrenean Thrust Belt is separated from the Axial Zone by a narrow region of deformed Carboniferous to Triassic sediments known as the Nogueres Zone. This zone is believed to represent the southern limb of a major antiformal stack of the southern Axial Zone (fig. 3; Séguret, ms, 1972; Muñoz and others, 1986; Vergés, 1999).

EXHUMATION OF THE PYRENEES FROM THERMOCHRONOLOGY

Here, we aim to document the relative timings and amounts of exhumation across the ECORS line of the Pyrenees (figs. 2 and 3) using low temperature thermochronology from the basement massifs of the Axial and North Pyrenean Zones. There is no evidence for normal faulting through this part of the orogen, therefore, we assume all exhumation to equate to erosional unroofing. We do not emphasize absolute exhumation rates as there is little constraint on the evolving palaeotopographies during exhumation that is likely to have resulted in a dynamic and unresolvable thermal structure of the shallow crust (Stüwe and others, 1994). This is particularly valid when the data plots with little age variance against elevation indicating rapid cooling associated with deformed isotherms (for example, Braun, 2003), as has been demonstrated for parts of the Pyrenees (Fitzgerald and others, 1999).

Apatite and zircon fission track (AFT and ZFT) data are presented and integrated with data from Fitzgerald and others (1999), Yelland (ms, 1991) and Morris and others (1998). In addition to the published sub-vertical profiles from the western Maladeta, Riberot and Lacourt Massifs (fig. 2; Fitzgerald and others, 1999), we provide new apatite and zircon ages from the eastern Maladeta, Nogueres Zone, Barruera and Marimaña Massifs (figs. 2 and 3).

Methodology for new data.—Three of the transects collected were from the Hercynian-age eastern Maladeta (from 2870 –1750m), Marimaña (from 2030 – 2635m) and

Barruera (from 1150 –1780m) granodioritic massifs from coherent structural blocks where no evidence was seen for significant faults or shear structures (fig. 2). The other transect from the Nogueres Zone was taken from the Carboniferous Erill Castell Volcanics (from 960 – 1280m) located north-east of Tremp (fig. 2). Individual samples were extracted from unweathered bedrock outcrop displaying no evidence of late-stage hydrothermal activity. The sampling strategy was chosen to cover the maximum possible elevation difference and the minimum horizontal deviation at each locality (fig. 2). The preparation and processing of samples was carried out at Apatite to Zircon Inc., USA by Ray Donelick; the procedures used are outlined in the caption to table 1. To compliment cooling ages, the cooling histories are analysed from Apatite track length distributions using AFTSolve (Ketcham and others, 2000). AFTSolve is a fission track-specific, numerical-based model that can be used to generate statistically-plausible T-t histories from a given suite of fission track data (for example, AFT age, track length distributions and kinetic data (dpar). The generated T-t histories are a function of the suite of data provided, the kinetic model imposed and the searching algorithm used.

Results and interpretations (eastern Maladeta, Marimaña, Barruera Massifs and Nogueres Zone).—The eastern Maladeta Massif data is plotted against the western Maladeta age profile from Fitzgerald and others (1999) for comparison (fig. 4B). The new data from 2870 to 1750m are within error of similar elevation samples from the western end of the Massif (20 km away). This assures us that we can compare the data from our study to the previous analyses by Fitzgerald and others (1999). The new samples comprise long track length distributions (13.7 – 14.27 microns) with low standard deviations (1.1 – 1.7). The age/elevation profile for the western Maladeta reveals no significant variation in age from 1945 to 2850 m with ages clustered around 32 Ma, and with confined mean track lengths ranging from 13.8 to 14.4 microns. This part of the profile has been interpreted as recording rapid cooling through the PAZ at approximately 32 Ma (Fitzgerald and others, 1999). Integrating the two datasets, it appears that the entire Maladeta Massif experienced a similar history of rapid cooling at approximately 32 Ma. The lower part of the western profile shows a kink from the upper part of the section, with a decrease in age with elevation, and with lower confined mean track lengths. These data have been interpreted to represent the preservation of the upper part of a PAZ that was established soon after the 32 Ma episode (Fitzgerald and others, 1999).

In addition to the AFT data we have obtained a ZFT age of 49.3 ± 2.6 Ma for the middle part of the Maladeta profile at 1760m elevation (fig. 4B; table 1). This puts a limit on the amount of denudation that can have occurred around 32 Ma, that is, it did not exhume material from below the zircon fission track closure temperature. In summary, the Maladeta Massif cooled from a depth below the ZFT closure temperature at, or before 49 Ma, and rapidly cooled through the AFT partial annealing zone at 32 Ma prior to a deceleration immediately after this.

The samples from the Marimaña Massif range in elevation from 2635 to 2030 m and in age from 36 ± 3.2 Ma to 27.6 ± 2.4Ma (fig. 4D, table 1). Confined mean track lengths for all the samples range from 14.19 to 14.32 microns with low standard deviations (1 – 1.58), which indicates steady cooling through the PAZ without any extended residency. Even though the age scatter with elevation is large, a regression line through the age/elevation profile is very steep to vertical supporting rapid cooling of all samples through the PAZ during the period 30 to 35 Ma. The ZFT age for the topmost sample of the Marimaña profile is 49.7 ± 3.1 Ma indicating that the massif was being cooled through the ZFT closure temperature during Middle Eocene times. The simplest interpretation of these data is that they represent a very similar cooling history to the Maladeta Massif.

The most southerly of the sampled massifs of the Axial Zone is the Barruera Massif from which we have obtained three AFT ages at elevations from 1150 to 1780 m, and a ZFT age for the lowest sample. The three AFT ages show no significant variance with elevation, all clustered around 20 Ma (fig. 4C, table 1). Confined mean track lengths for the upper two samples are 13.95 and 14.17 microns, which combined with low standard deviations implies rapid transit through partial annealing temperatures. The lowermost sample has shorter mean track lengths (13.18 microns). When this track length distribution is modelled using AFTsolve, it suggests a slightly slower passage through the PAZ than the upper two samples. The ZFT age for the lower sample is 104 ± 7 Ma, indicating a Pre-Pyrenean cooling history. When these ages are compared to similar elevation samples from the Maladeta and Marimaña Massifs, it is clear that the Barruera Massif experienced a later cooling history, and that the total depths from which it cooled during Pyrenean orogenesis were significantly less.

The samples from the Nogueres Zone range in age from 26.2 ± 3.1 to 17.2 ± 3.4 Ma (fig. 4A, table 1). The mean track lengths for these samples range from 13.75 ± 0.2 to 14.76 ± 1.2 microns with standard deviations from 1.9 to 2.8 microns. The sample with the longest mean track lengths and highest standard deviation only had six tracks measured, and hence we cannot draw meaningful conclusions from it. A lower sample at 805m also provided a ZFT age of 159 ± 33 Ma. As with the Barruera Massif, these outcrops have not been exhumed from below the ZFT partial annealing zone during the Pyrenean orogeny. Their passage through the AFT partial annealing zone, appears to have been later, and slower than the Maladeta and Marimaña Massifs having shorter track lengths and higher standard deviations, Axial Zoneothers.

Summary of published data.—The most northerly of all AFT ages along the line of study is from near Foix in the northern Arize Massif (figs. 2 and 3). The published age of 106 ± 5 Ma represents the oldest AFT age along the traverse (Yelland, 1990). The age and the confined track length distribution indicate steady cooling through the partial annealing zone (PAZ) during Middle Cretaceous times, possibly linked to strike-slip movement between the Iberian and European plates at this time, but prior to collision (Morris and others, 1998).

The Lacourt profile from Fitzgerald and others (1999) ranges from 1048m to 470m in elevation, and comprises five samples that range in age from 55 ± 3 to 37 ± 1Ma (fig. 4). The Lacourt granite represents the westernmost part of the Arize Massif (fig. 2). Fitzgerald and others (1999) argue that the three ages in the middle of the Lacourt profile record accelerated cooling through a PAZ at approximately 50 Ma, with the anomalously young age at the base of the section representing fault movement. By integrating additional data from Yelland (ms, 1991) from the same massif, it is conceivable that the profile may also be interpreted to represent steady cooling through the PAZ between approximately 55 and 33 Ma (fig. 4). This interpretation would infer that the profile can be fit by a linear regression and does not require a significant change in slope. Modeling of the confined track length distributions for two of the low elevation samples at 500 and 520m suggests relatively steady cooling through the PAZ from approximately 45 to 20 Ma (Morris and others, 1998). Alternatively, as suggested by Fitzgerald and others (1999), the interval between 600 and 1000 m elevation may represent rapid cooling, with the lower samples recording the slowing and residence within a PAZ developed after 50 Ma. The AFT age/elevation plot for the Riberot Massif yields ages from 44 to 36 Ma over an elevation range from 2483 to 1340 m. These samples may be interpreted as a record of steady cooling from 44 to 36 Ma with a subsequent slowing since then (Fitzgerald and others, 1999). Alternatively, the data could also record an acceleration in cooling between 38 and 36 Ma; there is no distinction in the mean track lengths of these samples that might differentiate these possibilities.

TABLE 1

Fission track data

Sample ID	Elevation meters	Grid Ref.	Rho-S (x106)	Rho-I (x106)	Rho-D (x106)	No. xls	Q	Dpar µm	Dper µm	Pooled FT Age Ma	Tracks	Mean Length µm	Std Dev µm
Marimaña													
Apatite													
MM-02/2635	2635	3564 3106	0.346 (181)	2153 (1126)	3.546 (4176)	25	0.466	1.72	0.53	32.4±2.8	125	14.28±0.14	1.58
MM-02/2440	2440	3520 3064	0.319 (181)	1 747 (992)	3.538 (4176)	25	0.176	1.88	0.51	38.6±3.2	130	14.19±0.11	1 27
Mar-00/2304	2304	3480 3019	0.311 (147)	2.012 (951)	3.977 (4146)	24	0.175	1.86	0.41	34.9±3.6	136	14.19±0.12	1.37
Mar-00/2200	2200	3464 3007	0.265 (177)	2.166 (1447)	3.979 (4146)	25	0.079	1.81	0.41	27.6±2.4	201	14.28±0.09	1.21
Mar-00/2030	2030	3422 3007	0.256 (171)	1 825 (1218)	3.982 (4146)	24	0.838	1 77	0.41	31.7±2.8	201	14 32±0 07	1
Zircon													
MM-02/2635	2635	3564 3106	7.168 (812)	5.606 (635)	0.578 (4072)	20	0.021			49.7±3.1			
Maladeta													
Apatite													
Mai-00/2870	2870	3769 0914	0.171 (121)	1.176 (833)	4.019 (4146)	25	0.49	1.83	0.44	33.1±3.4	137	14.27±0.15	1.7
Mal-00/2250	2250	3631 0829	0.132 (108)	1.058(865)	4.016 (4146)	25	0.148	1.81	0.42	28.5±3.0	117	14.02±0.14	1.54
Mal-00/2030	2030	3513 1867	0.235 (160)	1.930 (1313)	4.005 (4146)	25	0.154	1.69	0.39	27.7±2.5	126	13.88±0.10	1.08
Mal-00/1750	1750	3483 0805	0.139 (107)	1 095 (844)	4.013 (4146)	24	0 546	1 84	0.43	28.96±3.1	53	13 73±0 18	1 33
Zircon													
Mal-00/1750	1750	3483 0805	8.175 (1240)	6.448 (978)	0.578 (4072)	20	0.004			49.3±2.6			
Barruera													
Apatite													
Bar-02/1780	1780	1990 0995	0.094 (37)	0.882 (347)	3.505 (4176)	17	0.296	1.82	0.52	21.2±3.7	41	13.95±0.29	1.8
Bar-02/1695	1695	1995 0987	0.108 (41)	1.100 (419)	3.513 (4176)	17	0.738	2.08	0.78	19.5±3.2	41	14.17±0.23	1.45
Bar-02/1150	1150	2032 0925	0.265 (146)	2482 (1366)	3.521 (4176)	24	0.473	1.78	0.55	21.4±2.0	126	13.18±0.15	1.69
Zircon													
Bar-02/1150	1150	2032 0925	18.023 (1165)	6.730 (435)	0.578 (4072)	16	0.056			104±7			
Nogueres													
Apatite													
Mon-02/1280	1280	4290 9445	0.181 (86)	1.357 (646)	3.472 (4176)	25	0.37	2.08	0.67	26.2±3 .1	118	13.75±0.21	2.23
Mon-02/1085	1085	4335 9460	0.183 (45)	1.481 (365)	3.480 (4176)	25	0.876	1.93	0.55	24.4±3 .9	81	13.99±0.21	1.91
Mon-02/960	960	4365 9475	0.201 (29)	2.326 (335)	3.489 (4176)	9	0.005	1.97	0.56	17.2±3.4	6	14.76±1.23	2.76
Zircon													
Mon-02/805	805	4400 9495	16.146 (124)	3.906 (30)	0.578 (4072)	3	0.139			159±33			

TABLE 1
(continued)

All fission track slides were prepared and analyzed at Apatite to Zircon, Inc, USA. Apatite crystals were separated from the host rock using standard magnetic and gravimetric differentiation techniques and then mounted in epoxide resin and cured for 1 hour at 90°C. Internal crystal surfaces were exposed using 0.3μm Al_2O_3 slurries on a polishing wheel. Spontaneous fission tracks intersecting the polished surface were then etched in 5.5N HNO_3 for 20 seconds (±0.5) at 21°C and densities counted using both reflected and unpolarized transmitted light at 1562.5x magnification. For apatite track-length analysis the grain mounts were irradiated with ^{252}Cf-derived fission fragments in a nominal vacuum chamber to maximize track-length distribution measurements following the procedure of Donelick and Miller (1991). After re-etching, as outlined above, the length and crystallographic orientation, with respect to the c-axis, of natural, horizontal confined track lengths was determined under 1562.5x magnification with attached projection tube and digitizing tablet. Fission track ages were determined by placing low-uranium muscovite sheets against the polished and etched grain mounts prior to irradiation at the Washington State University nuclear reactor (45 minutes at thermal neutron fluence of 10^{16} neutrons/cm^2 at 1MW power level; position D9). Similar mica sheets were placed next to ^{235}U-doped CN-1glass for standardization purposes. The mica sheets were immersed in 48% HF at 20°C (±1°C) for 15 minutes (±15 seconds) in order to reveal fission tracks induced through irradiation. Fission track ages were calculated using the radioactive decay equation with an analyst zeta calibration factor of 113.8±2.9. Annealing kinetics were inferred using the arithmetic mean of 1-4 measured Dpar values (μm units) per grain. Quantitative analysis of the elemental composition of representative crystals from the same samples used for fission track analysis were determined to be Fluorapatites. This was achieved using the Backscatter Electron Detector method (20keV and 10mm working distance) and Energy Dispersive Spectrometry (EDS) and a PGT Spirit X-Ray analysis System. Rho-S and Rho-I are the spontaneous and induced track densities measured (tracks cm^{-2}). The bracketed numbers are the numbers of spontaneous and induced tracks counted. Rho-D is the induced track density in the external detector adjacent to the CN-1 glass. Bracketed is the number of tracks counted in determining Rho-D.

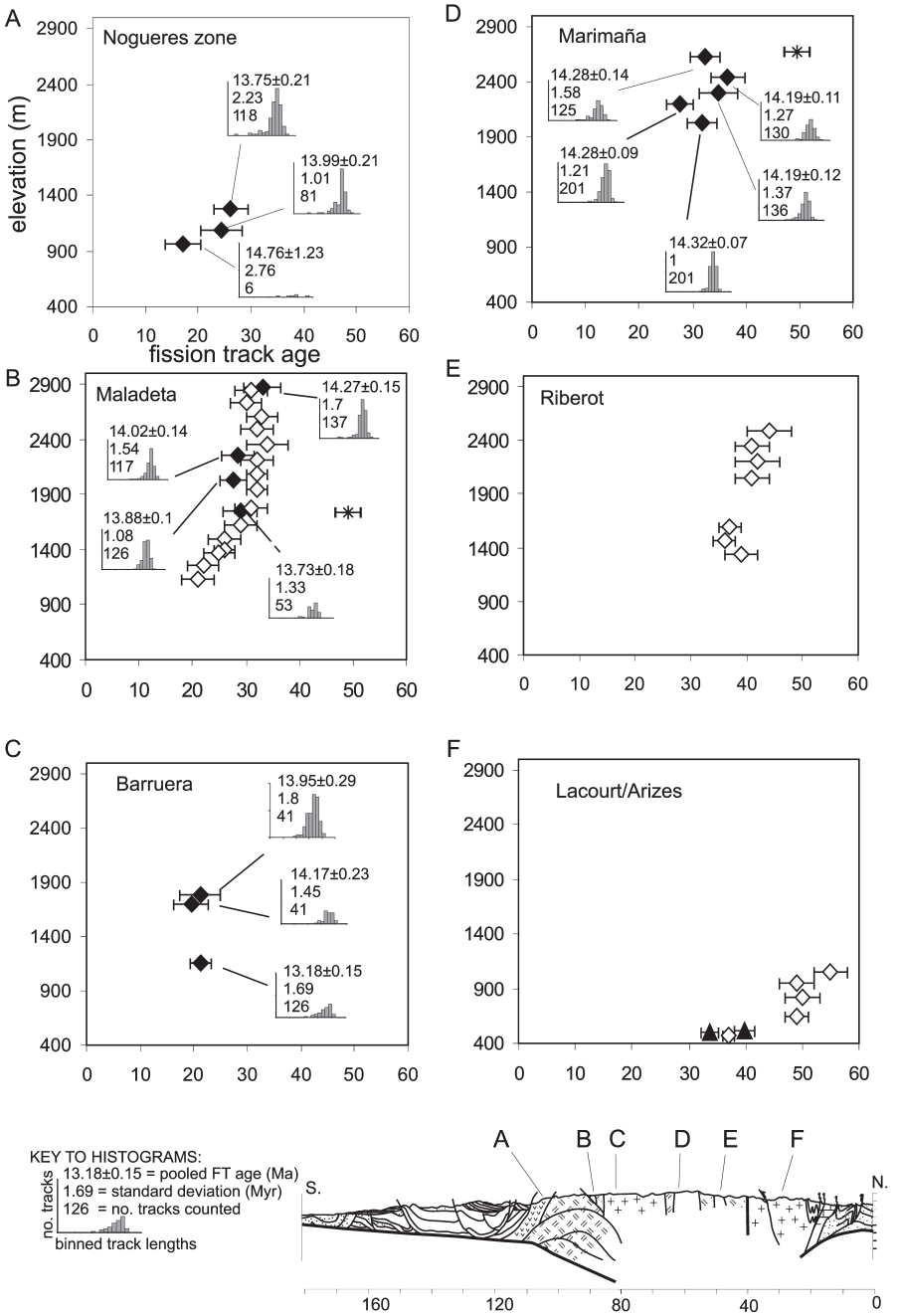

Fig. 4. Age/elevation plots for apatite and zircon fission track samples from the various locations shown in figure 2, and listed in table 1. Filled diamonds are new AFT data shown in table 1, empty diamonds are from Fitzgerald and others (1999). Starred data are new ZFT ages (table 1). Errors are ± 1 sigma.

Integration and interpretation of FT data.—Overall, these data demonstrate the asymmetric pattern of exhumation through time across the Pyrenees as recognized by Fitzgerald and others (1999). However, the integration of new data enables us to refine

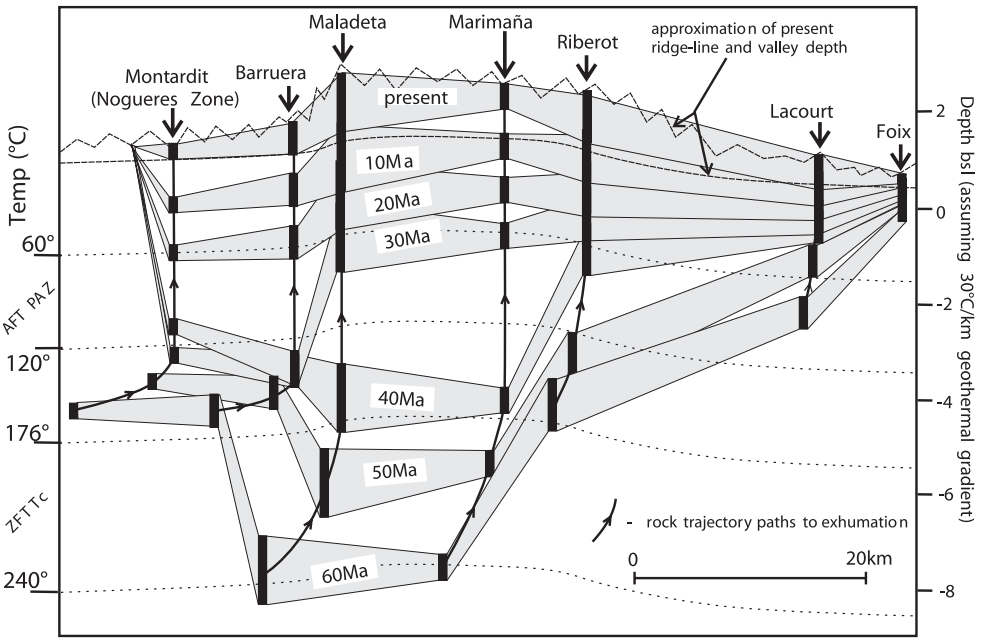

Fig. 5. Representation of relative cooling histories from the apatite partial annealing zone and zircon closure temperature for the sample sites projected onto a traverse across the Nogueres, Axial and North Pyrenean Zones. The isotherms are schematic to enable relative histories to be illustrated. The average valley and ridge heights are represented across this traverse to indicate first-order topographic form to which isotherms may have responded (for example Stüwe and others, 1994). The early history of cooling (60 – 50 Ma) was associated with extensive frontal accretion onto the pro-wedge. Therefore, during these periods it is interpreted that there was a significant component of retro-ward advection of the rock, hence the curved trajectory paths. This horizontal component of motion is not quantitatively constrained here. See text for further discussion.

our understanding of this development (fig. 5). In order for us to describe the relative cooling histories, it is necessary to discuss some of the factors that influence the record of cooling and the assumptions required to make comparisons.

Firstly, as the first-order form of the topography is a limiting control on the form of the isotherms, ideally, we would model the growth of the topography through time. However, as there are no available independent constraints on the topographic evolution of the orogen, we assume that at the time of mineral closure, the large-scale morphology of the mountain belt, in terms of mean elevations and the location of the drainage divide, approximated that of the modern system. Models suggest that topographic steady-state is achieved rapidly during the early growth of an orogen (Batt and Braun, 1997; Willett and others, 2001). However, this system has had approximately 20 Myr of post-orogenic erosion, which may have modified the original tectonically-driven form of the orogen.

Secondly, we assume that the isothermal surfaces that define the thermochronometric closure temperatures and partial annealing-/partial retention zones have remained broadly parallel to the mean long wavelength topography across the mountain belt. Local perturbations of the thermal regime from this parallel geometry are assumed not to exceed that which is likely imposed in the modern setting. That is to say, the amplitude and wavelength of the modern short-wavelength topography in the central Axial Zone is a broad approximation of the local topography during the time of mineral closure, and therefore topographically-induced isothermal perturbations are

also similar for a given set of uplift rates and thermal parameters. We also assume the advective influences of increased rates of exhumation on the thermal regime did not increase local geothermal gradients significantly. By applying these assumptions and employing the calculations of Stüwe and Hintermüller (2000), it can be shown that the magnitude of the topographic relief within the modern Pyrenean setting would induce perturbations of less than approximately 125m on the 110°C isotherm (approximately T_c for the apatite fission track system). These calculations are based on a maximum exhumation rate of 2 $kmMyr^{-1}$ in a steady-state setting (thermal diffusivity (K): 31.536 km^2Myr^{-1}, depth (L) and temperature (TL) of the lower boundary: 100km and 1000°C, respectively, Uplift rate (U): 2 $kmMyr^{-1}$, Wavelength (I) and Amplitude (H) of topography: 8 and 1.2 km, respectively). In addition, this estimation of isothermal perturbation must be considered a maximum value as it is based upon a two-dimensional representation of infinitely linear valley-ridge topography. In reality, the three-dimensional 'peak' topography of the region would have significantly less ability to perturb isotherms (Stüwe and Hintermüller, 2000; Reiners and others, 2003). The consequences of adopting an overly simplistic approach, and therefore poorly characterizing the true nature of isothermal deformation at the time of closure, have been shown to be significant when attempting to derive rates of exhumation from thermochronological data (for example, Braun, 2002), but of limited impact when assessing the relative variations in exhumation between specific localities, as in this study.

Finally, rock trajectory paths through the closure isotherms should also be considered when interpreting isotope chronology (for example, Batt and Brandon, 2002). As is documented later, the Pyrenees appear to have been dominated by a combination of frontal accretion and underplating in the early stages of development, with underplating dominating the accretionary flux later in the orogens development. While frontal accretion encourages horizontal advection of rock particles through an orogen, underplating translates material more vertically to the surface; hence, these processes represent first-order controls on the distribution of thermochronometric ages across an orogen (Batt and others, 2001).

The maximum depths of exhumation occur in the region of the Marimaña and Maladeta Massifs where Pyrenean age ZFT ages are found indicating erosional unroofing during latest Paleocene to early Eocene times (fig. 5). From Middle to Late Eocene times (approx. 50 to 40 Ma) the entire orogen from the Maladeta Massif north to the Lacourt Massif was unroofing; this represents the most rapid period of erosion for the Riberot Massif. By early Oligocene times (36 to 32 Ma) the more southern portion of the Axial Zone was rapidly eroding, with the cooling of the Marimaña and Maladeta Massifs through the AFT partial annealing zone; this was followed by an abrupt deceleration at approximately 32 Ma. The Nogueres Zone on the southern limb of the antiformal stack passed through the AFT partial annealing zone between approximately 26 and 17 Ma, and the Barruera Massif reveals the youngest period of cooling with erosion of the core of the evolving antiformal stack at 20 Ma. Given that this 20 Ma age is localized to the core of the antiformal stack, this indicates that the structure was still active at this time, and hence this extends the duration of Pyrenean orogenesis which had previously thought to have ceased at 30 Ma based on AFT ages (Fitzgerald and others, 1999) and approximately 26 Ma based on deformation of sediments in the Sierras Marginales (Meigs and others, 1996). This younger age for orogenesis compliments Iberia/Europe convergence histories from magnetic anomalies in the Bay of Biscay (Roest and Srivastava, 1991).

The southernmost boundary of the evolving antiformal stack is marked by the accumulation of syn-tectonic conglomerates that draped the edge of the previously deformed Nogueres Zone from 42 Ma to at least 24 Ma (Mellere, 1993; Beamud and others, 2003). We can therefore identify an abrupt southern boundary to the eroded

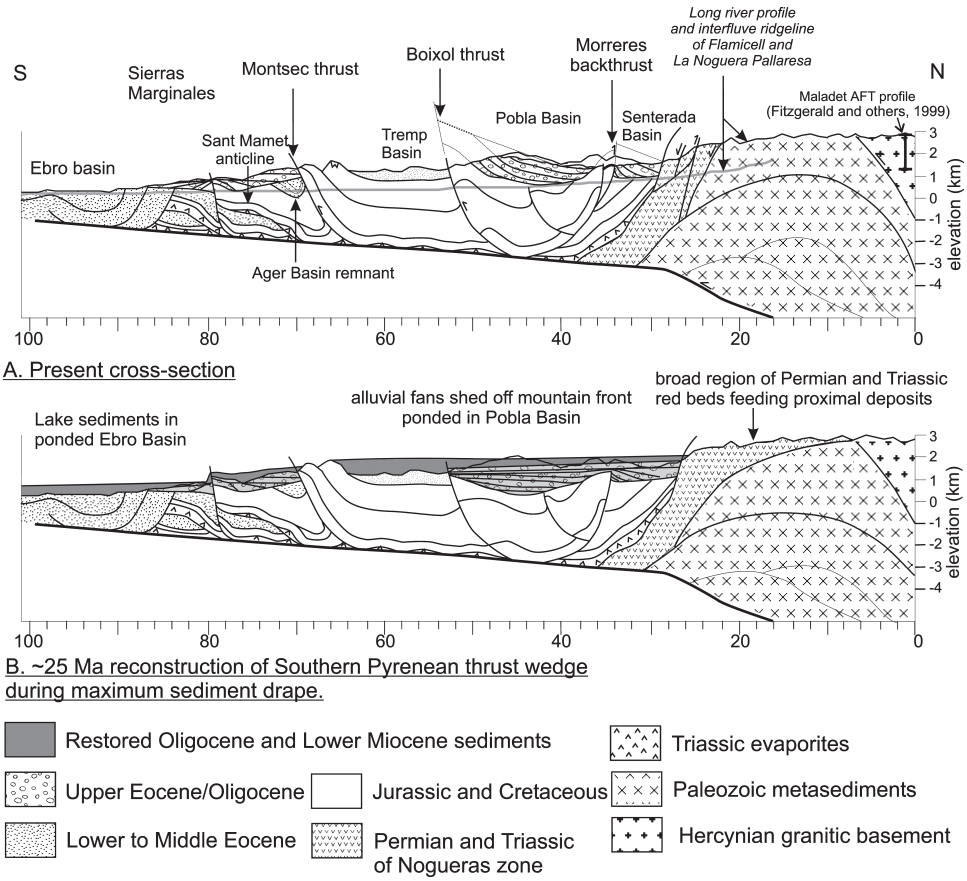

Fig. 6. (A) Cross-section through South Pyrenean Thrust Belt with river profile shown down the Flamicell and Noguera Pallaresa valleys, and interfluve ridges projected onto section enabling maximum information on syn-tectonic sediment drape. (B) Section restores to approximately 25 Ma to show the nature of the Oligocene to Miocene sediment drape over the South Pyrenees Thrust Belt.

antiformal stack during this time (figs. 2 and 6). The northern boundary is marked by the pre-Pyrenean AFT age given by the Arize Massif in the vicinity of Foix (Yelland, 1990).

In summary, the erosional unroofing of the core of the Pyrenean orogen evolved from a broad region of unroofing from 60 to 40 Ma, followed by a progressive southward shift with a period of highest erosion rates between approximately 36 and 20 Ma linked to growth of the antiformal stack. The data from Maladeta and Marimaña indicate that erosion of the northern limb of the antiformal stack decelerated soon after 32 Ma, but the southern limb, around the Nogueres Zone continued to erode after 26 Ma. This was followed by a tightening of the structure with erosion localized to its core at approximately 20 Ma. In considering the trajectory paths through the isotherms, frontal accretion was significant until approximately mid-Eocene times (see subsequent section), since which time, underplating dominated the accretionary flux. Therefore, horizontal advection of rock through the orogen is not considered to have played a major role in the Late Eocene to Miocene cooling of the Axial Zone.

The ZFT ages for the Maladeta and Marimaña Massifs suggest approximately 6 to 9.5 km of erosion over the core of the Axial Zone since 50 Ma; this assumes average

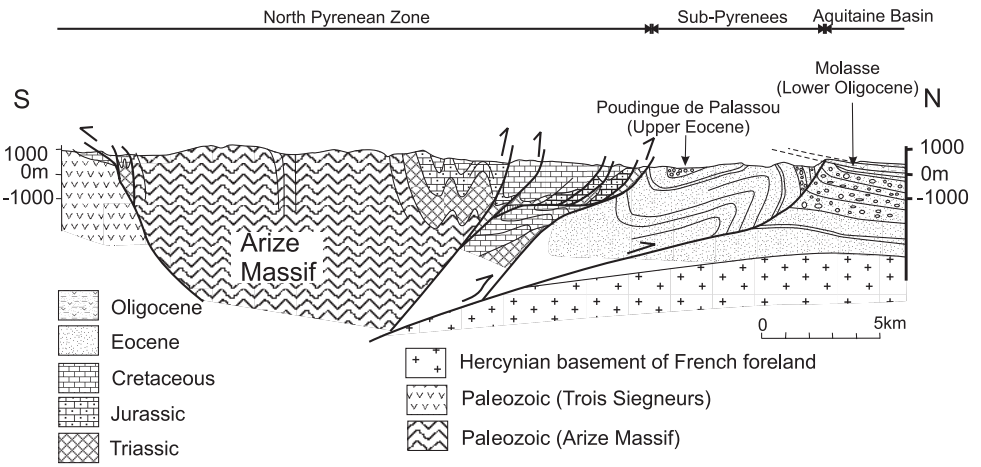

Fig. 7. Cross-section through the North Pyrenean Zone and Sub-Pyrenees demonstrating the timing of movement on the Sub-Pyrenean thrust front by the deformation of the Upper Eocene Poudingue de Palassou and the subsequent drape by the Lower Oligocene Molasse deposits of the Aquitaine Basin (modified from BRGM 1973).

geothermal gradients of 25 to 30°C/km (present-day values = 30°C/km; Zeyen and Fernández, 1994) and a ZFT closure isotherm of 176 to 240°C (Brandon and others, 1998; Bernet and others, 2002). This compliments, and places further constraints on previous estimates of the amounts of erosion based on balanced cross-sections (Vergés and others, 1995).

THRUSTING AND WEDGE-TOP SEDIMENTATION

Methodology.—Documenting rates of frontal accretion to thrust wedges using foreland basin strata has been achieved in a number of different settings (for example, Oriel and Armstrong, 1966; Jordan, 1981; Wilschko and Dorr, 1983; Homewood and others, 1986). In the southern Pyrenees, excellent preservation of syn-tectonic sediments has enabled a wealth of information on rates of thrust accretion using growth strata around evolving thrust anticlines (for example, Mellere, 1993; Williams and others, 1998) and truncation and onlap geometries of dated sediments around thrust faults (for example, Meigs and others, 1996). In many of the studies in the southern Pyrenees, detailed magnetostratigraphy has enabled relatively accurate dating of thrust-related folding in the Eocene and Oligocene strata (for example, Burbank and others, 1992). For this study, we build on the extensive research that has already been carried out along the line of the ECORS deep seismic profile (Choukroune and others, 1989). The timing of frontal accretion in the southern Pyrenees along the ECORS line has been documented by Meigs and others (1996) and Meigs and Burbank (1997). Here, we further develop this by incorporating new magnetostratigraphic ages from Beamud and others (2003) for conglomerates that blanket some of the more internal structures of the South Pyrenean Thrust Belt (fig. 6), and integrate this with data from the Sub-Pyrenees representing accretion to the northern retro-wedge (fig. 7).

South Pyrenean Thrust Belt.—The South Pyrenean Thrust Belt in the transect running through Balaguer and Tremp (figs. 3 and 6), comprises three main south-directed thrust sheets that detach in Triassic evaporites, and carry thick Mesozoic carbonates and Palaeogene siliciclastic rocks in their hanging-walls. These three thrusts are the Boixols, Montsec and Sierras Marginales (Séguret, ms, 1972; Muñoz and others, 1986; Muñoz, 1992). The northern-most thrust sheet (Boixols) is bound to

the north by a northwardly-vergent backthrust termed the Morreres backthrust (Mellere, 1993). This structure marks the boundary between the fold and thrust belt and the Nogueres Zone, which comprises Permian and Triassic strata wrapped around the Axial Zone antiformal stack (fig. 3; Séguret, ms, 1972; Muñoz, 1992).

The timing of initial movement on the three main thrust sheets is well documented. The oldest structure in this region is the Boixols thrust and the associated Sant Cornelli anticline located east of Tremp (fig. 2). Lower Cretaceous strata show a dramatic southward thickening into the hanging wall of the Boixols thrust indicating that it represents an inverted normal fault (Deramond and others, 1993). Upper Cretaceous and Paleocene strata thin and onlap onto the southern limb of the Sant Cornelli anticline and show associated intraformational unconformities and growth strata (Mutti and Sgavetti, 1987; Deramond and others, 1993). Similar stratal relationships are seen in the Upper Eocene sections of the Pobla de Segur Conglomerates that overlie the northern hanging-wall of the Sant Cornelli anticline (Mellere, 1993; Beamud and others, 2003). Therefore, the Boixols Thrust and Sant Cornelli Anticline were initiated in Late Cretaceous times, and were intermittently active until at least Late Eocene times. Deformation after this time is possible on these structures, as all of the Pobla De Segur Conglomerates are tilted by approximately 20° to the north in the hanging-wall of the Boixols thrust (fig. 6).

The Montsec thrust sheet forms a prominent ridge of steeply dipping Jurassic and Cretaceous Limestones (fig. 6). During Eocene times, this formed the structural boundary between the shallow marine Tremp and Ager basins to the north and south of the structure respectively (Mutti and others, 1985). The Figols Group that is seen to thicken away from the southern footwall of the Montsec thrust is middle Ypresian in age (53 – 51.5Ma; Mutti and others, 1988). Similar thickening of the Upper Paleocene Garumnian strata suggest that the Montsec thrust was initiated at this time (Vergés, 1999). Movement along the Montsec thrust terminated in late Eocene to early Oligocene times based on conglomerate drape over the structure as it is traced eastwards (Vergés and Muñoz, 1990).

The Sierras Marginales thrust sheet comprises a thinner Mesozoic succession relative to the Montsec and Boixols, and is emergent in the region north of Balaguer (Meigs and others, 1996; Vergés, 1999). The first evidence of activity on this structure comes from the Lower Eocene marine strata found between the Montsec thrust and the Sant Mamet anticline to the south which forms the hanging-wall of the Sierras Marginales thrust sheet (fig. 6; Vergés, 1999). The later history of movement on the Sierras Marginales thrust has been well documented for the interval 37.0 to 27.8 Ma using magnetostratigraphic dating of the surrounding continental sediments. From 37.0 to 29.5 Ma, the thrust sheet is interpreted to have been displaced stably over the footwall succession for approximately 30 km (Meigs and Burbank, 1997; Vergés, 1999). The intraformational unconformities between the time equivalent growth strata are angular and therefore record periods of erosion above emergent structures at the thrust front during, and immediately after this period of stable sliding (Meigs and others, 1996). An anticline in the footwall of the Sierras Marginales thrust to the east (the Oliana anticline) has associated growth strata that reveal steady deformation through this time period (Vergés, 1999) supporting the interpretation that the frontal thrust must have been sliding during this interval, and that it was emergent. Since 29.5 Ma there has only been approximately 1.2 km shortening to the south of the Sierras Marginales thrust sheet on relatively minor structures such as the Cubells backthrust and the Barbastro anticline (Meigs and Burbank, 1997).

The documentation of the timing of movements on the Boixols, Montsec and Sierras Marginales thrusts enable us to plot shortening across the South Pyrenean Thrust Wedge through time (fig. 8). If this is integrated with information on the

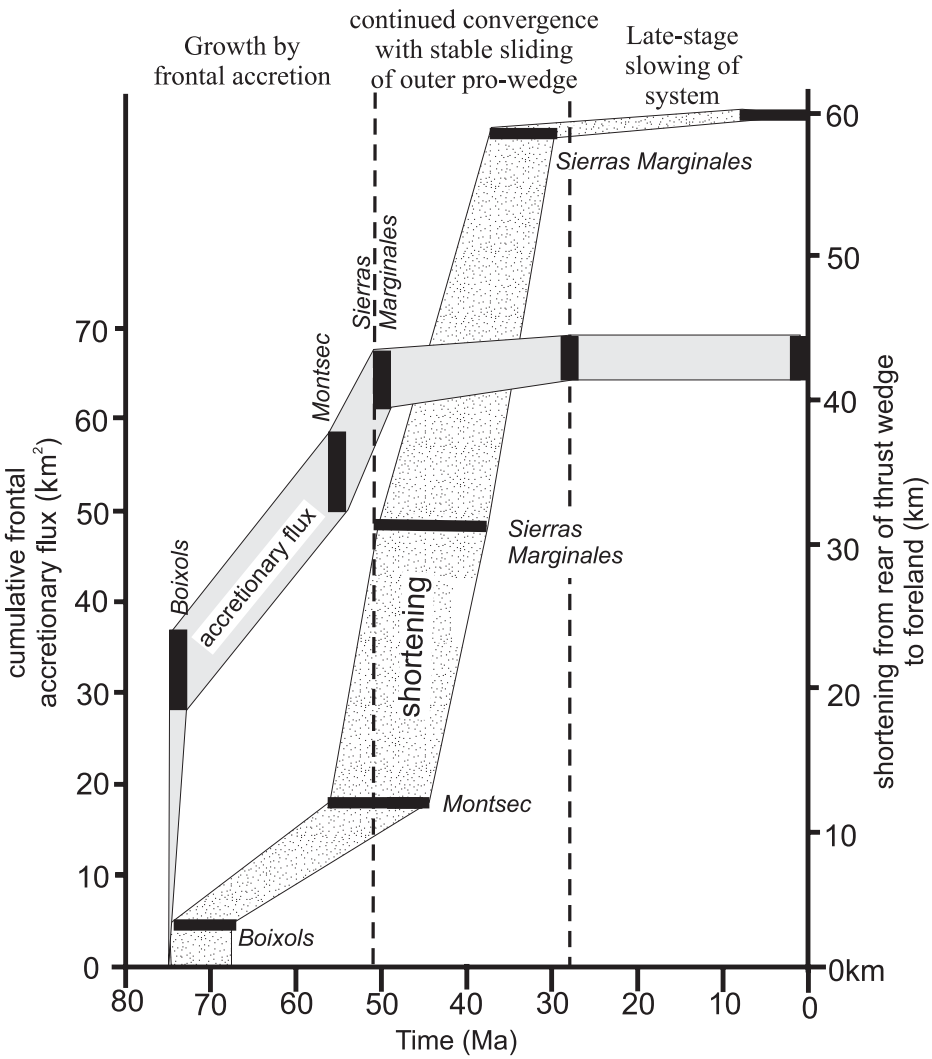

Fig. 8. Thrust shortening and accretionary flux of the South Pyrenean thrust Wedge plotted through time. Shortening amounts are taken as the amount of shortening across the South Pyrenean Thrust Belt from a point in the uppermost thrust sheet (Boixols) to a point in the undeformed foreland craton. The data are compiled from Specht and others (1991), Meigs and Burbank (1997) and Vergés (1999). The frontal accretionary flux was generated from a restored cross-section by Vergés (1999). The cumulative cross-sectional area for each of the restored thrust sheets was measured and plotted against the timing of initiation of the thrust sheet. The evolution of the South Pyrenean Thust Belt is divided into three stages: 1) Initial rapid growth by frontal accretion during which the wedge accreted the thick succession of the Boixols and Montsec sheets, and the relatively thin Sierras Marginales sheet. 2) Rapid shortening accommodated by stable sliding of the wedge over the underthrust foreland. During this interval there was little to no internal deformation or frontal accretion. 3) Slowing of convergent shortening during late-stage orogenesis.

restored thickness of the thrusted units that were incorporated into the thrust wedge (Vergés, 1999), then it is also possible to assess the mass flux of frontally accreted material into the pro-wedge of the Pyrenees. During the period from when thrusting was initiated approximately 75 Ma to approximately 50 Ma, the rate of mass flux through frontal accretion on the southern pro-wedge was approximately 1 km^2/Myr,

and shortening rates were approximately 0.6 km/Myr (fig. 5). After approximately 50 Ma (that is after initial accretion of the Sierras Marginales thrust sheet), the rate of frontal accretion was negligible with only a few minor structures developing in the foreland. However, the shortening rate accommodated through stable sliding over the underthrust foreland craton remained high from 1.3 to 4.8 km/Myr (Meigs and others, 1996). This period of stable sliding lasted until the slowing of the Sierras Marginales sheet at 29.5 Ma, after which there was only minor shortening across structures in the foreland. In summary, whilst localized deformation of the South Pyrenean Thrust Belt continued to the end of Oligocene times (approx. 30 Ma), the significant flux into the orogen from frontal accretion was achieved by approximately 50 Ma.

Sub-Pyrenees.—Accretion to the northern retro-wedge of the Pyrenees is represented by a thin-skinned fold and thrust belt that forms a narrow strip of deformed foreland basin sediments of Eocene age termed the Sub- Pyrenees (fig. 7; BRGM, 1973). These are bound to the north by the Sub-Pyrenean Thrust Front, and to the south by the North Pyrenean Thrust Front that carries thick Mesozoic successions dominated by the Cretaceous Flysch beds (fig. 3; see section below on Aquitaine Basin). Within the hanging-wall of the North Pyrenean Thrust are the Arize and Trois Seigneur Massifs for which three apatite fission track ages of 34, 38 and 39 Ma have been measured (Yelland, 1990). These ages indicate erosional unroofing at this time and can be interpreted as a record of thrusting on the North Pyrenean Thrust; whilst this gives us an age of activity on the structure, it does not yield a timing of initiation. The Sub-Pyrenean Thrust deforms a thick succession of Eocene strata, with the Upper Eocene Poudingue de Palassou capping the succession (BRGM, 1973; Mirouse, 1992). Draping over these defomed Eocene strata are Lower Oligocene 'molasse' deposits (BRGM, 1973; fig. 7). Hence this structure was initiated post-late Eocene times, and terminated prior to early Oligocene times.

FORELAND BASIN SEDIMENTATION

Aquitaine Basin.—The Aquitaine Basin was initiated by rifting in early Permian times, which continued episodically until Early Cretaceous times (Bourrouilh and others, 1995). Initial Permian fluvial sediments were overlain by up to 1000m of Triassic evaporites, then by up to 3500 m of Jurassic to middle Cretaceous limestones and mudstones. Throughout Cretaceous times, the Triassic salts were remobilized along faults to form diapirs that modified basin morphology. During late Early Cretaceous times, rapid, localized subsidence occurred in a number of pull-apart basins, and sub-basins developed containing thick accumulations of deep-water siliciclastics in their lows, and carbonate growth on the faulted highs. By Cenomanian times, surface uplift along the North Pyrenean Fault generated an emergent landmass that provided sediment for the basins of the North Pyrenean Trough that ran immediately north of the present-day North Pyrenean Fault (Bourrouilh and others, 1995). This style of sedimentation continued until end-Paleocene times and resulted in the accumulation of up to 5000m of "North Pyrenean Flysch".

This history of fault-block development formed the template upon which the Tertiary succession accumulated. Consequently, the Tertiary Aquitaine basin has been divided into a series of sub-basins (the Parentis, Arzacq, Mirande, Tarbes and Comminges sub-basins) bound by inherited structural highs termed shoals (fig. 9A). Throughout Paleocene and early Eocene times, calcareous turbidites and marls accumulated in the North Pyrenean trough. An abrupt change took place in Middle Eocene times when shallowing and the deposition of thick conglomerates along the southern fringes of the Aquitaine Basin took place. The conglomerates (Poudingues de Palassou) are intercalated with nodular mudstones and sandstones, and suggest

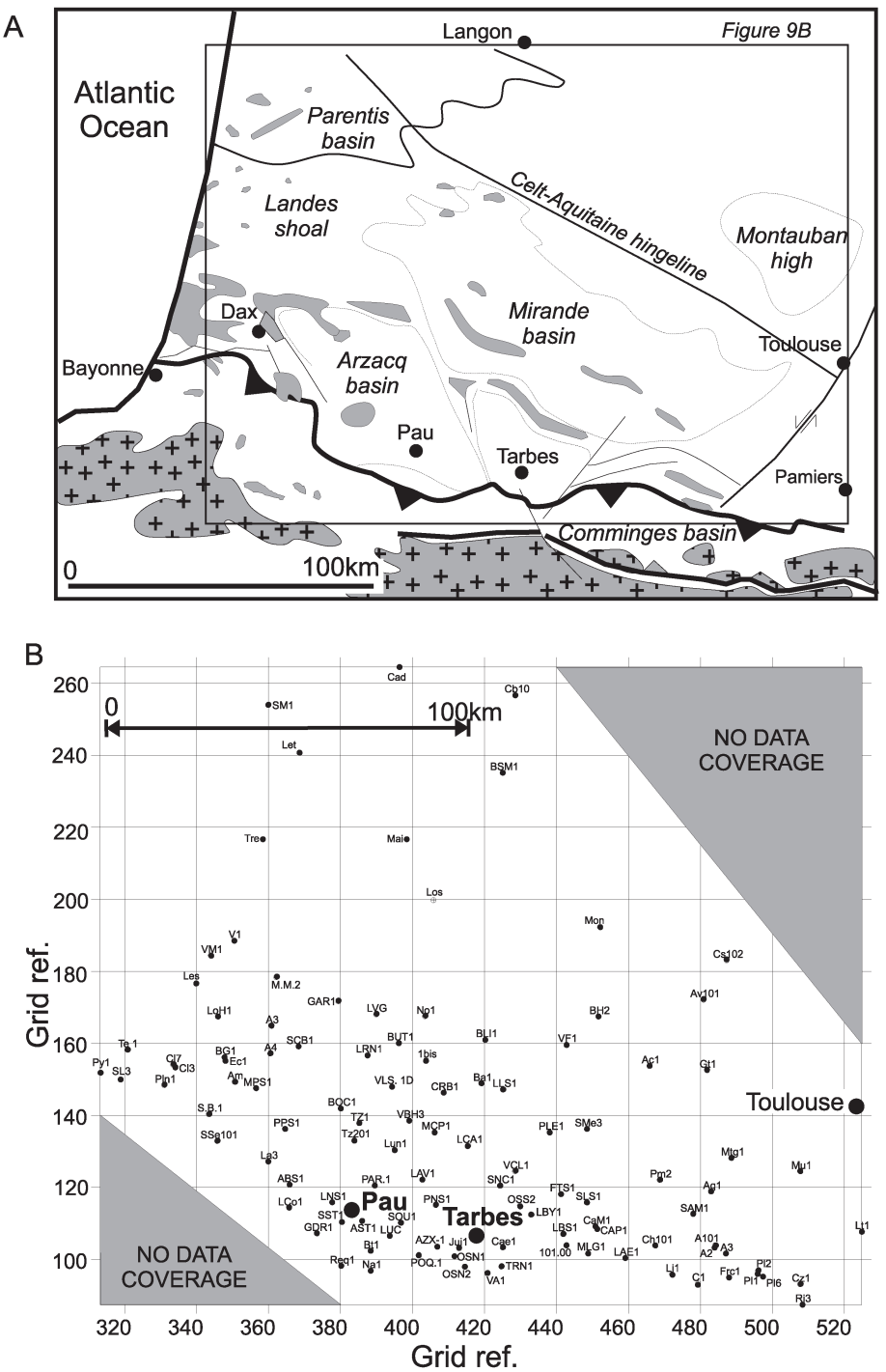

Fig. 9. (A) Geological map of the Aquitaine Basin showing the location of intra-basinal highs and the sampling region shown in B. (B) Names and locations of the wells used in the construction of the isopachs illustrated in figure 10. Well names and grid reference system are those given by the Ministère de l'Industrie de la Poste et des Télécommunications.

fluvial settings with periodic marine transgressions (BRGM 1973). Molasse sedimentation continued in the southern Aquitaine Basin up to Pliocene times.

In order to evaluate the volume of sediment preserved in the Aquitaine Basin through the Tertiary, isopach maps were generated for specific intervals (fig. 9B). These maps are generated from 105 wells acquired from the Ministère de l'Industrie de la Poste et des Télécommunications (Service de Conservation des Gisements d'Hydrocarbures) for the region west of Toulouse to the Atlantic Ocean. As most of the flow within the basin was westward into the Atlantic, it is intended that this region records a representative history of evolving sedimentation rates. Thicknesses for the stratigraphic intervals for the Danian, Upper Paleocene, Ypresian, Lutetian, Upper Eocene, Oligocene and Miocene were recorded. However, because a large number of the wells do not differentiate the Oligocene and Miocene succession, we have also integrated them. For each interval a thickness value was assigned to each well, and the region was contoured using a Kriging method. The isopach maps were converted into volumes of rock that were then divided by the time interval of accumulation, the area over which they accumulated, and a rock density of 2500 kg m^{-3} to yield sedimentation rates in mm/yr.

The isopach maps reveal a complex pattern of sediment accumulation across the basin. Initial accumulation through Paleocene times (Danian and Thanetian; fig. 10) was focussed in the Tarbes and Arzacq sub-basins. The Tarbes sub-basin continued to act as the main depocentre from Upper Paleocene to Lower Eocene (Ypresian) times. During the Paleocene and Lower Eocene, overall mean sedimentation rates through the sampled region accelerated from 0.02 to 0.05 mm/yr. Middle Eocene times recorded a westward shift in the locus of sedimentation into the Arzacq sub-basin, and a reduction in sedimentation rates to 0.02 mm/yr. From Upper Eocene times onwards, sedimentation occurred dominantly in the south and east of the region at rates similar to those during the previous intervals (fig. 10). These results are used for comparison to the Ebro Basin, although it is recognized that some of the sediment produced from the northern Pyrenees is likely to have been flushed into the Atlantic of the Bay of Biscay.

Ebro Foreland Basin.—The Ebro foreland basin has a broadly triangular shape bound to the north by the Pyrenees, to the southeast by the Catalan Coastal Ranges, and to the southwest by the Iberian Ranges (fig. 1). The basin is a direct response to crustal loading by all three of these ranges, but is dominated by the Pyrenees (Brunet, 1986; Desegaulx and others, 1990; Zoetemeijer and others, 1990). Much of the tectono-stratigraphic development of the Ebro Basin is best recorded in syn-tectonic wedge-top basins of the south Pyrenean fold and thrust belt and well data from the undeformed foredeep (Puigdefàbregas and others, 1986; Puigdefàbregas and Souquet, 1986; Puigdefàbregas and others, 1992). Subsidence in the basin was initiated in the north-northwest in the position of the present-day fold and thrust belt, and migrated south-southeastwards through time (Vergés and others, 1998). The stratigraphic history of the basin has been divided into four phases (Puigdefàbregas and others, 1992): 1. Late Santonian to Maastrichtian accumulation of turbidites in deep troughs that developed during inversion of Lower Cretaceous extensional faults in the northern part of the basin (see earlier discussion of Boixols thrust history). 2. Late Maastrichtian to Paleocene transition into continental red beds in the north, with deep-water carbonates towards the west. 3. Early to Middle Eocene turbidite sedimentation in east-west aligned basins with time equivalent carbonates accumulating to the south in the present-day center of the basin. 4. Late Eocene to Miocene infilling of the turbidite troughs with deltaic, fluvial and alluvial sediments, and a transition from longitudinal discharge to transverse south away from the mountain belt. Sedimenta-

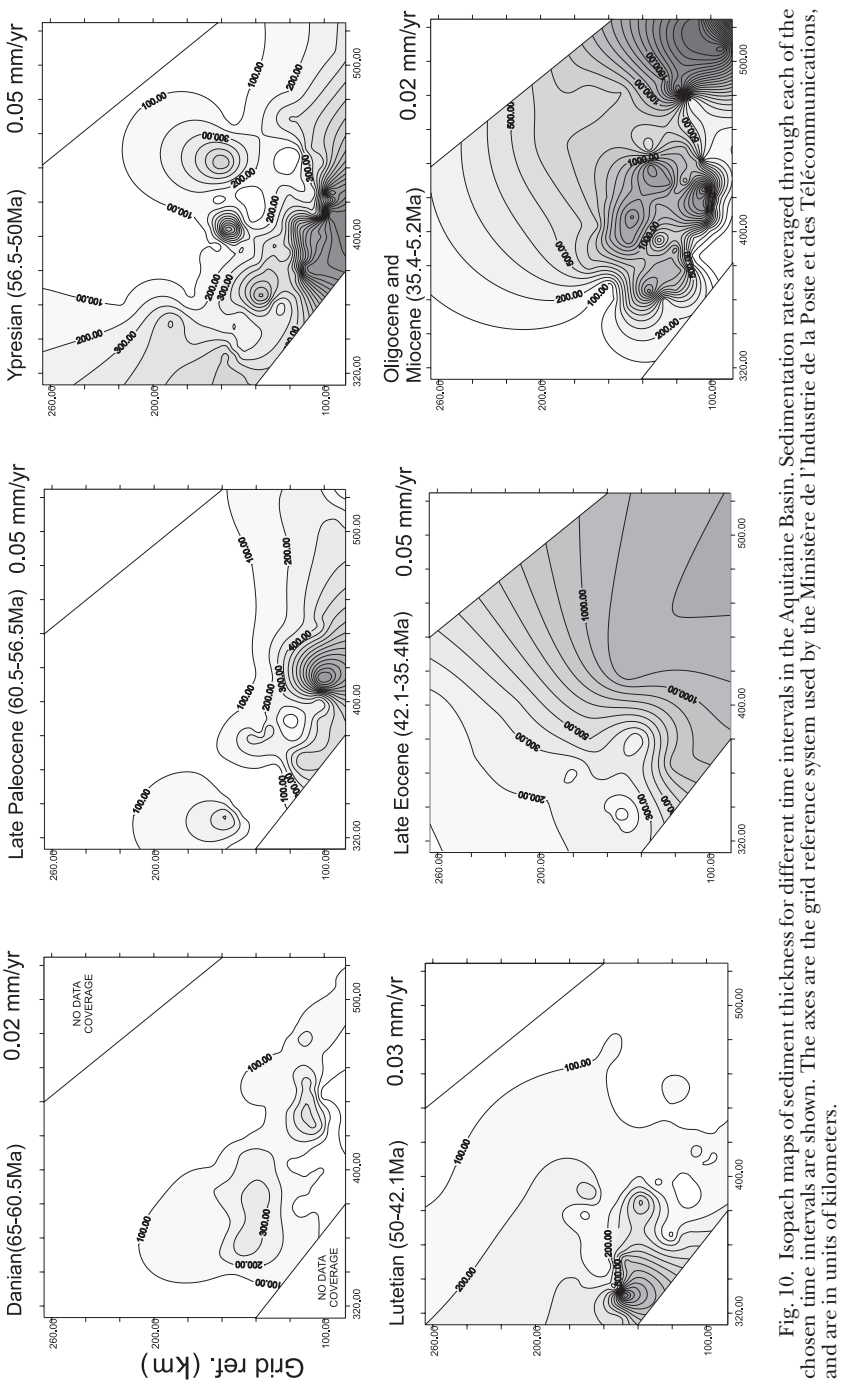

Fig. 10. Isopach maps of sediment thickness for different time intervals in the Aquitaine Basin. Sedimentation rates averaged through each of the chosen time intervals are shown. The axes are the grid reference system used by the Ministère de l'Industrie de la Poste et des Télécommunications, and are in units of kilometers.

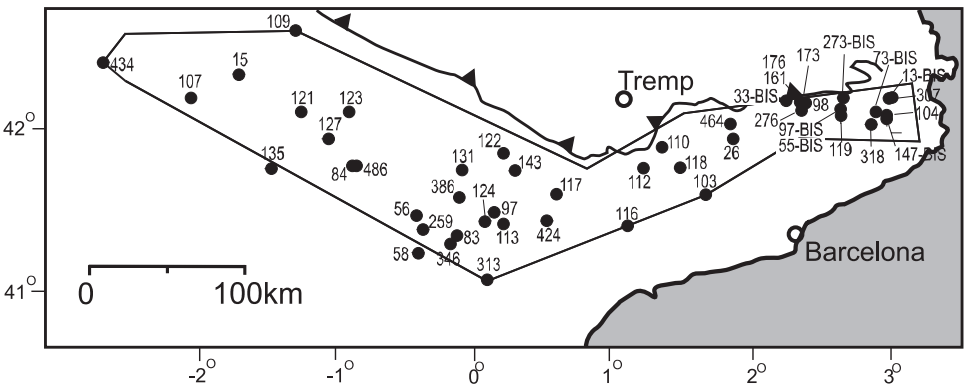

Fig. 11. Well locations in the Ebro Basin used in construction of the isopachs shown in figure 12. Names link to those given in Lanaja and others (1987).

tion continued with underformed lacustrine and alluvial sediments up to at least 14 Ma in the center of the basin (Pérez-Rivarés and others, 2002).

These youngest lacustrine and fluvial sediments of the Ebro Basin are preserved undeformed at current elevations of 800m (Pérez-Rivarés and others, 2002). The youngest sediments preserved in the Pobla Basin (the most orogen-ward of the wedge-top basins) are approximately 24 Ma assuming steady sedimentation rates from the magnetostratigraphically dated underlying succession (Beamud and others, 2003). These sediments are preserved at elevations of approximately 1700m onlapping onto the margins of the Nogueres Zone (Coney and others, 1996). These observations have led some workers to suggest that the Ebro Basin was ponded, caused by structural confinement by the Catalan Coastal Ranges and the Iberian Ranges from uppermost Eocene to Miocene times (Riba and others, 1983; Coney and others, 1996). This sediment ponding has been interpreted as the driver for blanketing of the South Pyrenean Thrust Wedge by thick conglomerates from Late Eocene to mid Miocene times (figs. 3 and 5; Mellere, 1993; Coney and others, 1996; Beamud and others, 2003). However, it is important to note that the accumulation of continental conglomerates in the Pobla Basin occurred prior to the interpreted confinement of the Ebro Basin (Beamud and others, 2003). It is also important to recognize that there was a structural barrier between the Ebro Basin and the wedge-top basins as evidenced by the intraformational unconformities located around the Sierra Marginales thrust sheet (Meigs and others, 1996; see previous description).

Isopach maps for the bulk of the undeformed Ebro Basin were generated from 48 wells extracted from a compilation of Spanish well data (Lanaja and others, 1987; fig. 11). The sample area covered by the wells has avoided regions where provenance data indicate that there is evidence for significant volumes of material being derived from the Iberian Range and Catalan Coastal Ranges (Allen and Mange-Rajetsky, 1982; Villena and others, 1996; Teixell, 1998). However, these data do not incorporate regions where sediment is now incorporated into the thrust wedge, such as the Jaca Basin in the west, and in the northern flank of the Ripoll Basin in the east where up to 5 km of sub-vertical lower to middle Eocene strata are partially preserved (Vergés, 1999). Chronostratigraphic resolution in the wells permitted four temporal sub-divisions to be established, Ypresian, Lutetian, Upper Eocene and Oligocene. These intervals were correlated and isopach maps generated as with the Aquitaine Basin. Additionally, a complete Tertiary isopach map was generated (fig. 12) showing a general thickening of the basin succession northwards, and the presence of two primary depocenters; one

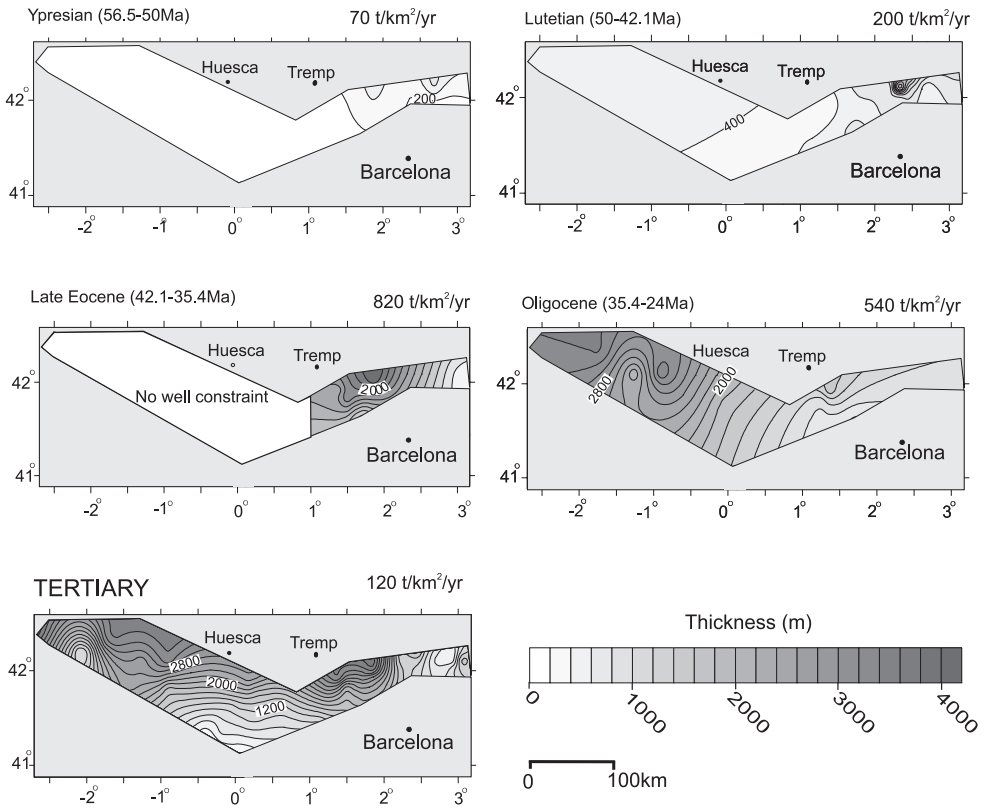

Fig. 12. Isopach maps for varying time intervals for the Ebro Basin with time averaged sedimentation rates labelled above each map.

located approximately 60 km east of Tremp, and the other in the west, approximately 50 km northwest of Luna (Anadón and Roca, 1996). This latter depocenter marks the easternmost end of the Rioja Trough (Muñoz-Jimenez and Casas-Sainz, 1997).

The isopachs for the four intra-Tertiary time intervals presented, reveal the initiation of thick sediment accumulation in the eastern part of the basin from Lutetian to Upper Eocene times, and that by Oligocene times, the thickest accumulations were in the west of the basin. Sedimentation rates increased from 0.03 mm/yr during Ypresian times to 0.08 mm/yr during Lutetian times, increasing again to values of 0.3 and 0.2 mm/yr for the Upper Eocene and Oligocene respectively (fig. 13). Clearly, these undeformed Ebro Basin sediments do not represent all the sediment produced from the southern Pyrenees at this time, as much sediment was preserved in wedge-top basins such as the Jaca and Ripoll Basins. Consequently, the sediment volumes for the early basin development will be minimum amounts. However, as with the Aquitaine Basin, the sampled region is sufficiently large to represent the major relative changes in sedimentation rates.

The increase in sedimentation rates in the Ebro Basin occurred prior to the interpreted closure of the basin, which is recorded by the transition from marine siliciclastic sediments of the Igualada Formation to the continental evaporites of the Cardona Formation in late to end Eocene times (Riba and others, 1983). The oldest conglomerates of the Pobla Basin are mid- to upper Eocene in age (42 Ma – Beamud

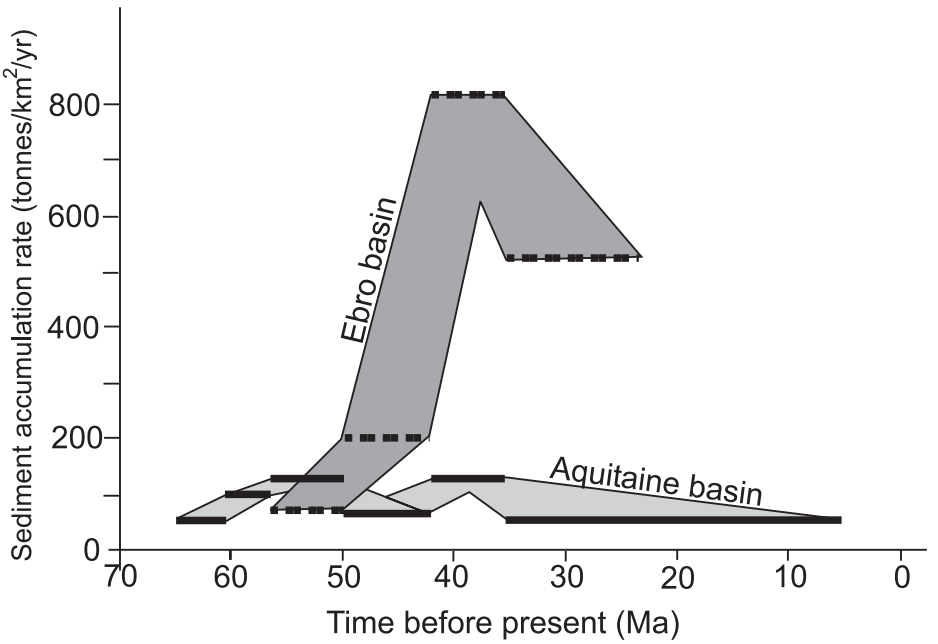

Fig. 13. Plot of sedimentation rates for the Ebro and Aquitaine Basins through time.

and others, 2003) indicating that the draping of the wedge was also initiated prior to the ponding of the Ebro Basin.

GROWTH OF THE PYRENEES—A QUALITATIVE INTERPRETATION

Summary of Pyrenean growth.—In order to compare the relative timing of the growth of the orogen through frontal accretion, underplating, erosion, and the consequent sediment yield to its foreland basins, it is necessary to plot these data together against time. Chronostratigraphic plots have been widely used to study the interactions of thrust faults with foreland basin stratigraphy (for example, Schedl and Wiltschko, 1984; DeCelles, 1984; Burbank and others, 1986). However, a plot of thrust development and foreland basin stratigraphy for both sides of an orogen has not previously been achieved, but has the potential to yield insight into coupling between the pro- and retro-wedge components. The difficulty in constructing a plot of this type is that the components of the system are moving in different directions and at different rates relative to each other through time. A point on the pro-plate moves towards the retro-plate at the overall convergence velocity until it is accreted into the wedge. When in the wedge, it moves more slowly, and intermittently towards the retro-plate depending on the incremental strain distribution within the wedge. A parcel of rock on the retro-plate is stationary in this frame of reference until it is accreted, and is then translated over the point at which it is accreted. In order to plot such complexity in a single frame of reference requires a reconstruction of the trajectory paths of every package of rock through the orogen with time. As yet this has not been achieved, and so we use separate frames of reference for the two sides of the orogen; those being stable points on the pro- and retro-plates. The division between these two frames of reference is a vertical line drawn above the restored position of the singularity. The restoration used for the pro-wedge was taken from Beaumont and others (2000), and integrated with new data for the retro-wedge (fig. 7). The absolute accuracy of the

restoration is not vital, as we are primarily concerned with relative motions and timings. Additionally, the area where we have the most accuracy is in the fold and thrust belts where frontal accretion is documented. The same plot is used to illustrate the timing of erosional denudation across the orogen, and sedimentation rates in the foreland basins. However, we must also recognize the dangers in comparing a two-dimensional reconstruction of erosion with three-dimensional sediment volumes in a foreland basin; inevitably, the erosion of the mountain belt will have varied along its strike. However, we are only extracting the first-order signals from these data (that is an order of magnitude increase in the Ebro).

The growth of the Pyrenees can be viewed in terms of four stages that have been recognized by previous workers (for example, Vergés and others, 1995; Beaumont and others, 2000) but that are revised here based on the new data provided (figs. 14 and 15):

1) Orogenesis started in Late Cretaceous times and was characterized by the localized development of structural highs over the Sant Cornelli and Turbon anticlines generated by transpressive deformation and inversion of normal faults (figs. 14 and 15). Sedimentation in both basins was marine, with turbidites infilling basinal lows, whilst the north-eastern Pyrenees were uplifted above sea-level (Puigdefàbregas and Souquet, 1986; Specht and others, 1991).
2) From end-Paleocene to mid-Eocene times (figs. 14 and 15), the system records steady unroofing of the Axial and North Pyrenean Zones; rapid frontal accretion onto the South Pyrenean Thrust Belt (pro-wedge); fully marine depocenters for both foreland basins with modest and comparable rates of sedimentation; initial sediment drape of pro-wedge by marine wedge-top basins (for example Tremp and Ager Basins).
3) During mid- to late Eocene times (figs. 14 and 15), accretion and internal thickening of the retro-wedge took place during a period of inactivity on the pro-wedge. It was also the period when the two foreland basins were filled to, or above sea-level.
4) From Oligocene to early Miocene times, the pro-wedge was reactivated by stable sliding over the foreland succession associated with rapid erosional unroofing of the southern Axial Zone linked to underplating and the growth of the antiformal stack. This growth generated a four-fold increase in sedimentation rates in the pro-foreland basin, and established the present-day structural form of the orogen (figs. 14 and 15).

EXPERIMENTS WITH A DISCRETE ELEMENT MODEL

Background to model.—We employ a 2D discrete element model developed by Naylor and others (2005) in order to investigate the natural progression of a doubly-vergent orogen. The aims of this component of the study are to assess the orogenic processes that are required to understand the primary aspects of the evolution of the Pyrenees as summarized in figure 15. The model localizes deformation across discrete faults as an emergent phenomenon in a similar way to sand-box experiments; this opens a new field of investigation, and hence provides a significant advance on previous numerical approaches (for example Beaumont and others, 1999).

Discrete element models were first developed by Cundall and Strack (1979) as a method for analyzing granular materials. The approach taken by Naylor and others (2005) uses large numbers of elements to approximate the rheology of deforming rock within an orogen. A spring-dashpot model limited by Coulomb failure is used to calculate contact forces between irregular elements. The size of these elements limits the scale of structure that can be resolved. We apply geologically motivated boundary conditions and then numerically integrate the resulting equations of motion. The rheology is an emergent property of the model and compares well with the orogen-

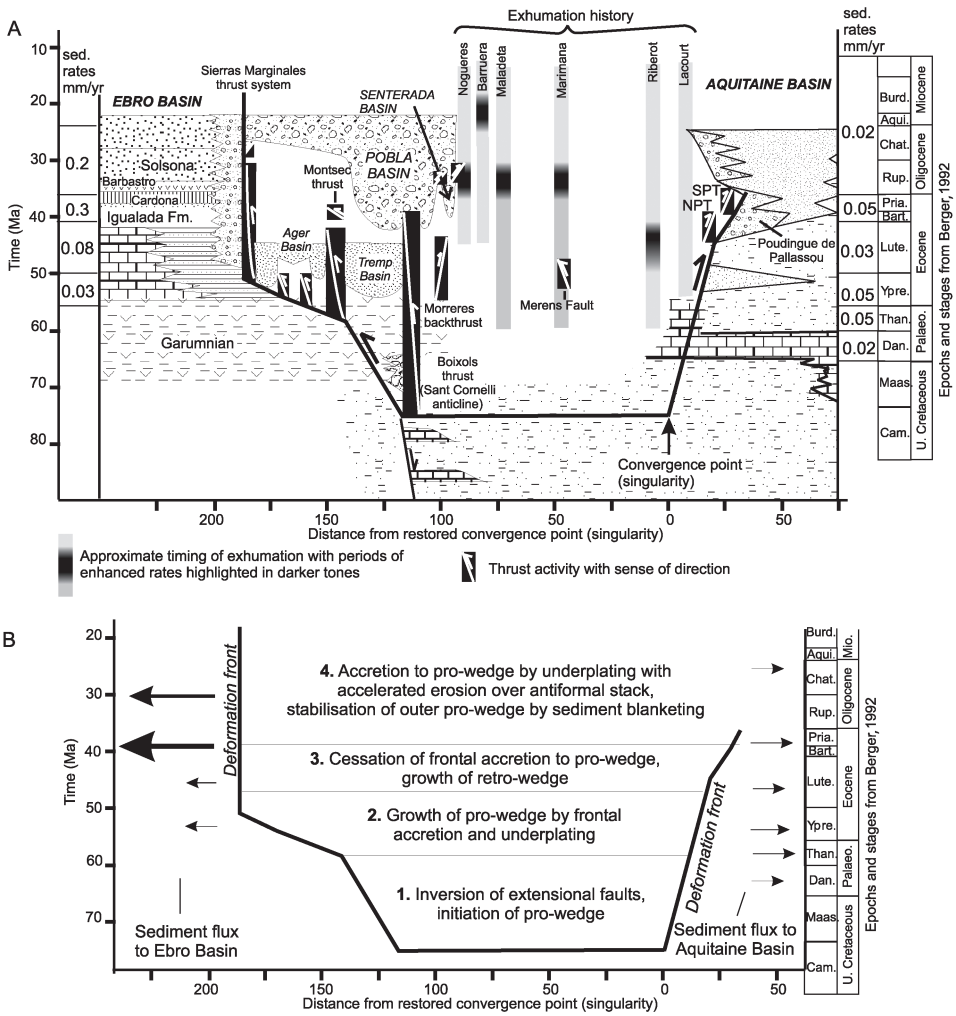

Fig. 14. (A) Chronostratigraphic plot documenting the timing of thrust shortening and the timing of erosional exhumation of the core of the orogen relative to the preserved stratigraphic record. The x-axis represents the distance from a restored convergence point based on the restorations of the Pyrenean orogen presented by Beaumont and others (2000). Separate frames of reference are used for the pro- and retro-wedges, and are points on their respective undeformed plates. Importantly, the propagation of the pro-wedge deformation front is not shown to move back into the orogen as illustrated in subsequent model output (fig. 17). Presently, we do not have the data on the amounts of internal shortening in the orogen that would permit integration of this component of the system. Stratigraphic data from the Ebro Basin is summarized from Vergés (1999) and Mutti and others (1988). Aquitaine Basin stratigraphy from Bourrouilh and others (1995). Thrust movement data from Specht and others (1991), Mellere (1993), Bond and McClay (1995), Meigs and Burbank (1997), Wayne and McCaig (1998), and derived from BRGM (1973). Fission track data presented here (table 1), integrated with data from Fitzgerald and others (1999). Chronostratigraphic timescale from Berger (1992). (B) Interpretational summary of the chronostratigraphic figure showing the four phases discussed in the text, and shown in figure 15.

scale behavior of the finite element models, but also permits localized strain down to the scale of individual thrust faults.

The distinction between the over-riding and the subducting plates of the model is made by introducing a discontinuity in the basal velocity on a Coulomb lower

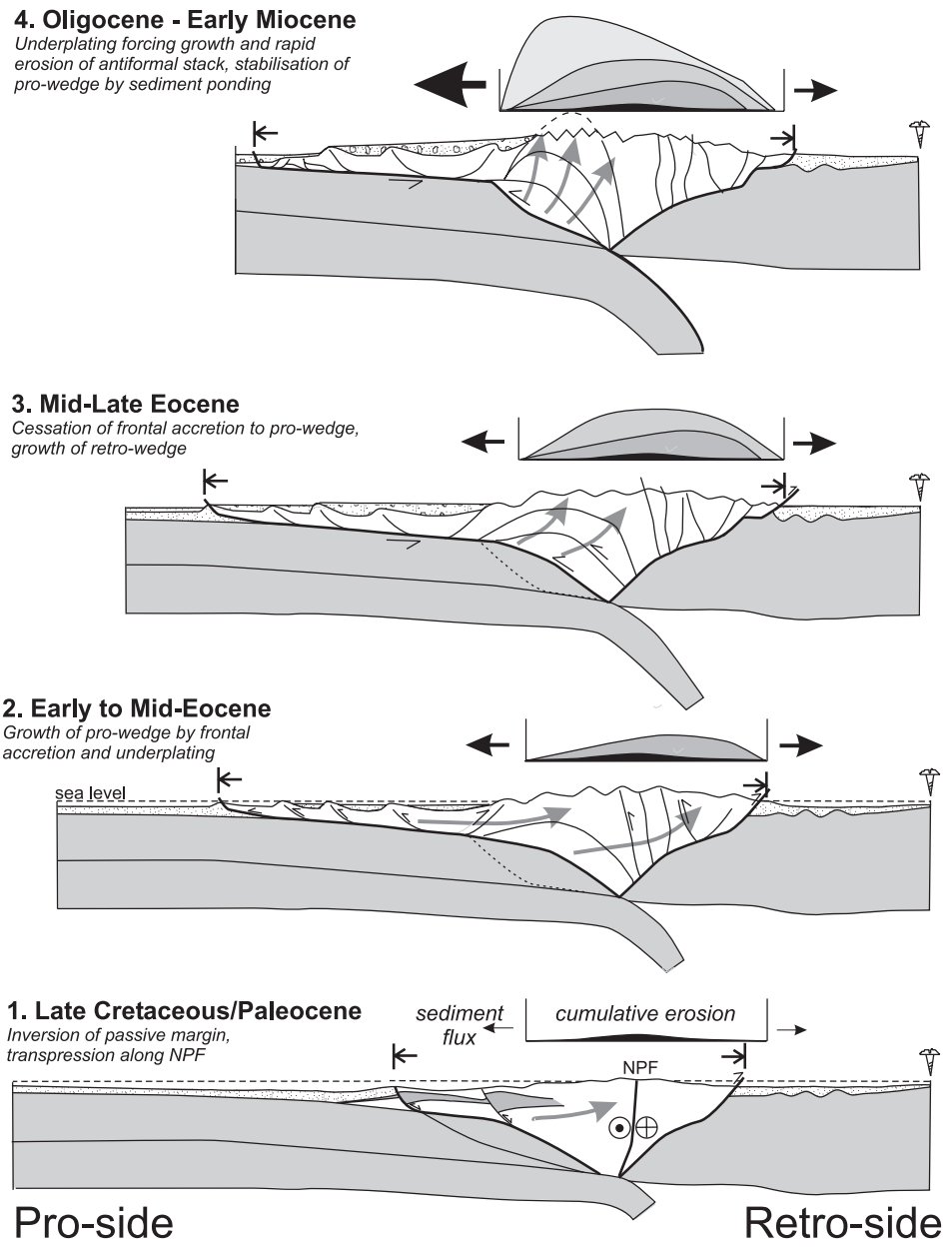

Fig. 15. Summary of the evolution of the Pyrenean orogen based on fluxes through the system recorded by frontal accretion, underplating, erosion and sedimentation. The four figures represent the four stages outlined in figure 14B and discussed in the text.

boundary; this discontinuity is termed the S-point. The lower boundary represents the line below which all material is subducted. Material on the over-riding plate is stationary with respect to the S-point, material on the under-thrust plate is dragged towards the S-point by a traction force derived from the lower boundary. As material thickens over the S-point during convergence a topography is developed that is

supported on an infinitely rigid plate. That is there is no isostatic compensation for topography incorporated into the model.

We examined the interaction of this system with a simple erosional algorithm that removed all material above a mean height. This represents a mean topographic elevation above which erosion is efficient at removing all material that attempts to surmount it. The material is removed from the model and not redeposited as sediment. The end result is that erosion responds directly to structurally-driven rock uplift rate above the threshold. The importance of this approach is that whilst simplistic, it is easily understandable in terms of the link to tectonic forcing as there are no lag times in response.

Three experiments were run with identical parameter combinations to describe the tectonic forcing of the system, but with either no erosion, erosion at a threshold 2 times the thickness of the accreted crust ($2.0T_c$), and with an erosional threshold at $1.5T_c$. The output for each model run starts with a series of images of the deforming discrete element wedges (figs. 16 A, B and C). For each output, we plot the progressive outward migration of the deformation fronts for the pro- and retro-wedges (fig. 17). In addition there is a plot of the cumulative erosion located over a snapshot of the final state of the erosional models showing short trajectory paths for the elements in the model (figs. 18A and B).

Model results.—The non-erosive model run illustrates the growth of the orogen through three distinctive stages (Willett and others, 1993; Naylor and others, 2005). Initially, convergence is taken up by a retro-vergent thrust that propagates up from the S-point forming a rise in topography (Stage 1). Subsequently, a detachment is formed at the base of the incoming succession, and pro-wedge accretion is initiated whilst the retro-wedge evolves by over-steepening (Stage 2). Finally, as the wedge grows it forces accretion of material onto the retro-wedge which decreases in slope (Stage 3). The lateral growth of the modeled orogen can be documented through a plot of the pro- and retro-deformation fronts away from the singularity (fig. 17). The averaged trend of these lines away from the singularity illustrates the power law decline (approximately $t^{0.5}$) in growth rate as the orogen grows in size. The irregular fluctuations around this trend illustrate the variability of activity on the deformation front as stress localization oscillates within the modeled orogen in order to maintain some form of mechanically stable morphology. The retro-wedge deformation front steps out with an irregular history over the uppermost plate. In contrast, the pro-wedge deformation front steps out during episodes of accretion, but is then dragged back into the orogen as the interior of the wedge thickens, and the pro-wedge taper angle increases. Thus, the width of the pro-wedge fluctuates around a long-term growth trend by increasing during episodes of accretion, and decreasing during periods of internal thickening as the deformation front is translated towards the interior of the orogen. The major episode of growth of the retro-wedge deformation front between 125 and 150 output timesteps, is coincident with a prolonged period of inactivity on the pro-wedge deformation front (fig. 17). This indicates that at that time, the entire orogen was being pushed over the upper plate, but that this is terminated when the stresses at the pro-wedge deformation front are released, and frontal accretion and growth of the pro-wedge is re-established.

The second experiment introduces a threshold for erosion at $2T_c$; this could be seen as a rough approximation of emergence from sea-level of a 2 km high thrust wedge into a super-efficient erosional regime, where the thickness of accreted material (T_c) is also 2 km. Similar changes in erosion with elevation can occur with intense orographic enhancement of precipitation (Roe and others, 2003), and with glacial erosion (Hallet and others, 1996). Figure 16B illustrates the initial growth of the wedge without erosion until output timestep 85 when the threshold is reached at the crest of

Fig. 16. Experimental output from the discrete element model (Naylor and others, 2005). The three experiments vary only in the approximation of erosion, with (A) representing the case of no erosion, (B) where an erosional threshold is set at an elevation twice the thickness of the incoming material (T_c), and (C) where the erosional threshold is placed at 1.5 times T_c. The impact for depths of exhumation, erosion and propagation of the deformation fronts for these experiments is shown in figures 17 and 18.

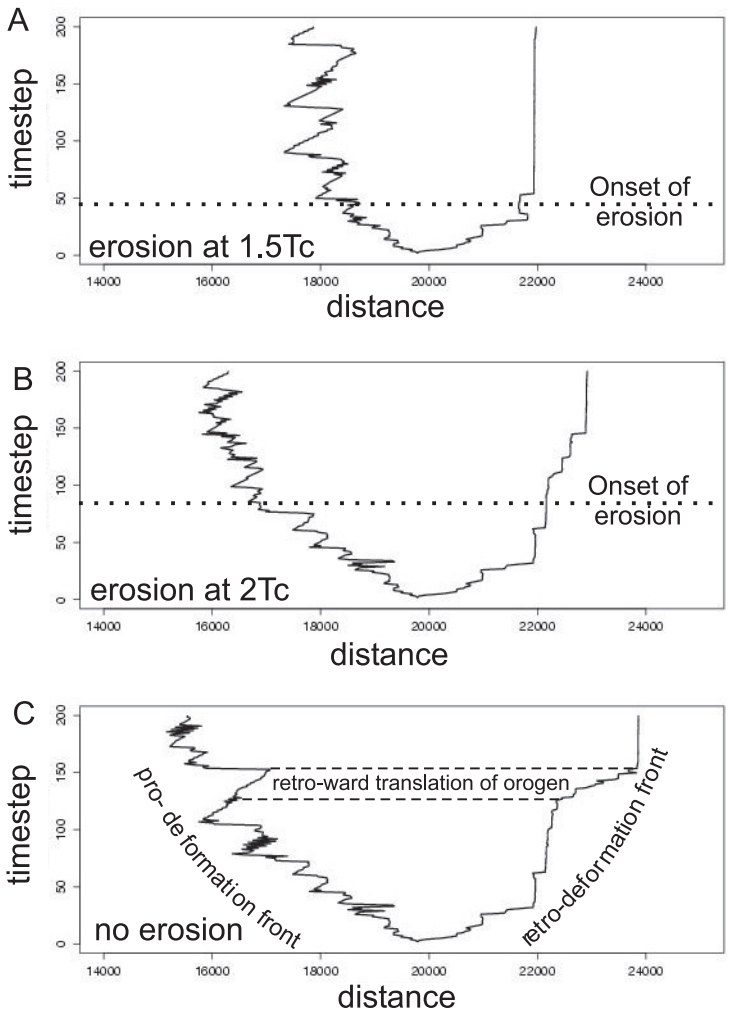

Fig. 17. Plot of deformation front propagation for the pro-and retro-wedges for the three experiments illustrated in figure 16. As erosional influence increases in the three experiments, so the long-term growth of the orogen decreases. With higher erosion, the convergence towards a time-averaged flux steady-state (Willett and Brandon, 2002) occurs more rapidly. The oscillation of the pro-deformation front reflects the fluctuation of the growth of the pro-wedge between episodes of frontal accretion, and periods of internal thickening; during the former, the deformation front moves outward, during the latter it is pulled back into the mountain belt. Note the motion of the retro-deformation front appears to respond to the locking of the pro-deformation front in the non-erosive case. This coupling decreases when trajectory paths are more upright during erosion, and would be decreased further if isostasy were introduced.

the deforming orogen. Figure 18 illustrates the progressive and cumulative erosion for five output timesteps. The irregular pattern of erosion is caused by the localization of structural-induced rock uplift in the interior of the modeled orogen. The initial erosion is located over the S-point, but shifts pro-wards with time as the orogen grows, resulting in a skewed distribution of total erosion towards the pro-side of the system. The particle vectors (fig. 18) demonstrate that the distribution of erosion is deter-

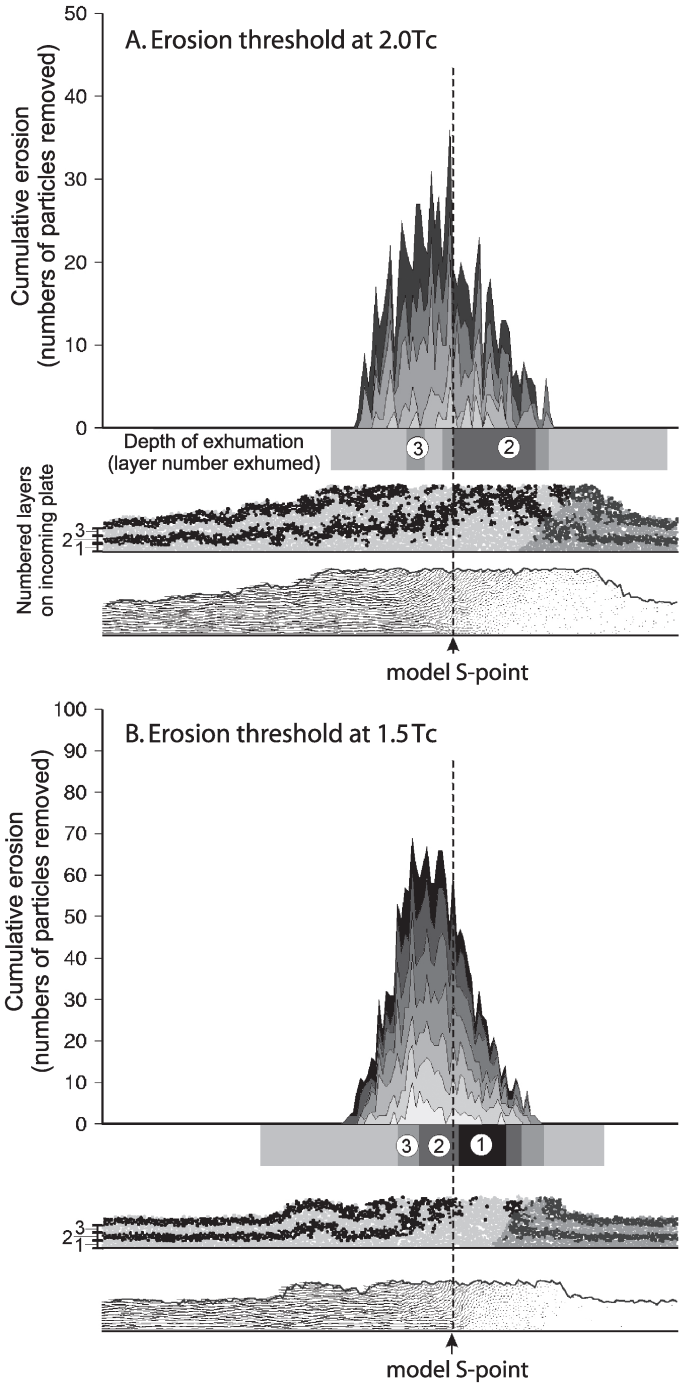

Fig. 18. Plots showing the distribution of erosion versus the depths of exhumation revealed by the two erosive models illustrated in figures 16 and 17. The lowest portion of each plot shows vectors for each particle during the last 3 time steps, and clearly demonstrates the reduction in particle velocities from the pro-wedge into the retro-wedge. The middle portion of the plots uses numbered bands to indicate the region over which exhumation depth has reached the numbered layers in the underlying particle plot. The uppermost portion illustrates the cumulative erosion over the model measured as the number of particles removed from

mined by the flux of material that originates at the deformation front and moves towards the upper surface of the pro-wedge. During this time the retro-wedge experiences little strain, effectively acting as a relatively inactive backstop. The plot depicting the motions of the deformation fronts during the growth of the system demonstrate the slowing in growth of the pro-wedge at the onset of surface erosion (fig. 17). The retro-wedge deformation front propagates over the upper plate in a series of steps through this interval.

The final experiment accentuates the erosional component by placing the threshold at 1.5 T_c. The run illustrates the localization of both erosional denudation and deformation in the interior of the orogen (fig. 16C). As with the $2T_c$ model, erosion is skewed towards the pro-wedge with particle vectors demonstrating the relative inactivity of the retro-wedge (fig. 18). The deformation fronts reach a time-averaged steady-state where there is no long-term growth of the orogen after approximately 80 output steps (fig. 17). During this interval, the pro-wedge deformation front continues to fluctuate about a stable mean due to fluctuating episodes of frontal accretion and internal thickening. The retro-wedge remains static for the bulk of the time due to the high flux of material from the accreting pro-wedge out through the upper erosional surface.

DISCUSSION OF MODEL RESULTS

Erosion and exhumation.—The experiments with the discrete element models illuminate the potential interactions between erosion and accretionary growth of an orogen. They do not attempt a simulation of the Pyrenees (compare Beaumont and others, 2000), but instead provide new insight into the natural evolution of accretionary wedges and orogens that enables a simpler interpretation of the Pyrenees.

The thermochronology from the Pyrenees and the sedimentation rates in the foreland basins indicate a shift in the focus of erosional exhumation towards the pro-wedge with time (fig. 5). The erosion experiments (figs. 16B and C) illustrate that the intense coupling between erosion and internal deformation in the pro-wedge is a natural tendency of the modeled system. This can be explained by recognizing that for a doubly-vergent wedge at taper, all material that is removed through erosion, will be replaced by tectonic deformation in order to retrieve taper. The rate at which material is replaced will vary spatially across the orogen in response to the progressive reduction in the horizontal velocity of particles from the pro-wedge deformation front to the retro-wedge deformation front. The result is a strong coupling between erosion and deformation that is greater on the pro-side of the orogen. This natural tendency for material flux to be greater on the pro-side of the orogen is a fundamental component of orogenesis that defines a strong asymmetry without recourse to spatial variations in the surface processes.

Numerous other studies have analyzed the distribution of long-term erosion across mountain belts. In the Olympic Mountains of Washington state, long-term erosion appears to be in a flux steady state, with maximum values skewed towards the pro-wedge (Brandon and others, 1998; Batt and others, 2001; Pazzaglia and Brandon, 2001). In contrast, maximum erosion rates in the Southern Alps of New Zealand are heavily biased towards the western side of the range, which is considered the retro-

---

that point. Note the offset towards the retro-side of the orogen in exhumation depth versus the amount of erosion. This is due to the rapid, and shallow trajectories of particles accreted to the pro-wedge deformation front, and eroded from the pro-wedge compared to the slow trajectories seen in the retro-wedge. This intense coupling between erosion and high strain in the inner parts of the pro-wedge approximates the processes of rapid accretionary flux through underplating and erosion over the antiformal stack of the Axial Zone in the Pyrenees during the final phase of growth (figs. 14 and 15).

wedge (Kamp and Tippett, 1993; Batt, 2001; Willett and Brandon, 2002). The pattern of erosion over mountain belts, incorporating asymmetry in precipitation has been investigated using finite element models (Willett, 1999). The output from these models has emphasized that the natural tendency of the system is for maximum depths of exhumation to occur in the region of the retro-wedge. Therefore, based on the continuum models, the Southern Alps would be viewed as the natural distribution of exhumation that has been enhanced by strong orographic asymmetry on the western side. In contrast, the Olympic Mountains have been viewed as a system that has countered the natural tectonic forcing by a marked orographic enhancement on the western pro-wedge (Willett, 1999).

While initially, the suggested predictions for the natural erosional tendency of the finite and discrete element models appear to contradict each other, they can be reconciled. The deformed finite element meshes remain intact and visible in the experiments after the material has been eroded away (for example Willett, 1999). Due to the strong component of horizontal advection of the finite element mesh it is difficult to determine where the erosion responsible for the exhumed material took place. However, the output of the finite element models have not been used to illustrate the distribution of erosion, instead revealing the depths of exhumation in order to predict measurable thermochronometric ages across orogens (for example Willett, 1999, his fig. 5B). In contrast, when comparing thermochronology with the spatial development of erosion and consequent sedimentation rates in foreland basins, there may be some discrepancies. The discrete element models reveal that a large proportion of material eroded from the pro-wedge is exhumed to the surface on low-angle trajectories that need not have dipped beneath the AFT closure isotherm (fig. 18). This flux of shallow crustal material is dependent upon the depth of detachment at the thrust front, the pro-wedge taper angle and the distribution of erosion. In contrast, trajectory paths in the retro-wedge are steep and come from greater depths in the wedge (fig. 18). Consequently, unreset, shallow crustal material in the retro-wedge can only be replaced by material that has originated from greater depth, and hence is directly linked to the depth of exhumation as recorded by thermochronology.

The potential discrepancy between the amounts of erosion and the depths of exhumation from a point on the pro-wedge may help us to understand the relative distribution of sediment to the foreland basins versus the thermochronometric age distributions in the Pyrenees. Pyrenean age ZFT dates, are centered in the Axial Zone (Maladeta and Marimaña Massifs - approx. 50 Ma). AFT ages younger than 50 Ma are found in the Nogueres Zone, the Axial Zone and the North Pyrenean Zone with the youngest ages centered around the antiformal stack on the southern edge of the Axial Zone that is on the pro-side of the orogen. The post 50 Ma sediment delivery was far greater to the pro-foreland basin (Ebro) than the retro-foreland basin (Aquitaine).

One possible explanation is that despite greater depths of exhumation through the center of the Axial Zone, erosion was greater towards the pro-side due to unreset shallow crustal fluxes during frontal accretion. However, the acceleration in sedimentation in the Ebro Basin occurred after the dominant period of frontal accretion in the Pyrenees, but synchronous to the growth of the antiformal stack induced by underplating. Therefore, the offset of young AFT ages and of sediment production towards the pro-wedge compared to the young ZFT ages can be explained by a transition from frontal accretion to underplating, that is from horizontal to more vertical trajectory paths. The other factor that may have been important is that the drainage divide may have been further north (retro-side) during active growth of the orogen as predicted by numerical models (Willett and others, 2001).

Propagation of thrust fronts.—The plots that record the modeled history of the deformation fronts for each experiment (fig. 18) have a different reference frame to that shown in figure 15. The modeled output is able to demonstrate the motion of both deformation fronts relative to a stable upper plate. Therefore, the pro-deformation front is able to illustrate both outward propagation during episodes of frontal accretion, and inward migration during periods of internal thickening. Because of the difficulty in defining the timing of internal deformation within the Pyrenean orogen we have chosen not to incorporate it by plotting the deformation fronts relative to their respective stable plates. Therefore, they do not show inward migration during periods of inactivity on the thrust fronts as is likely to have been the case.

The initial period of rapid frontal accretion during Paleocene and early Eocene times followed by a subsequent slowing is a general prediction of the model. However, the apparent cessation of frontal accretion and stable sliding of the pro-wedge during late Eocene and Oligocene times is not a prediction of any of the models. It is important to note that throughout the growth of the pro-wedge, thick accumulations of sediment were ponded in piggy-back basins. These accumulations were detached from the sediment of the Ebro foreland basin as evidenced by the intraformational unconformities above the Sierra Marginales. Therefore, these accumulations would have increased the surface slope of the thrust wedge, and driven it into a stable configuration (Willett, 1992). During stable sliding of the outer parts of the pro-wedge, the inner parts of the same wedge grew by underplating and formation of an antiformal stack.

Inherited extensional faults may well have played a significant role in the initiation of the Axial Zone thrust sheets (Muñoz, 1992; Vergés and others, 1995, 2002). However, heterogeneities in the underthrust plate are not required in order to explain the accelerated erosion and growth of the antiformal stack as has been suggested (Fitzgerald and others, 1999; Beaumont and others, 2000). Instead, this is a record of a dynamic coupling between continued underplating and an efficient erosional system in the interior of the pro-wedge.

Another outcome of the discrete element models is that cessation of pro-wedge frontal accretion promotes the likelihood of retro-wedge accretion as well as internal thickening (fig. 17). Retro-wedge accretion occurred during mid- to late Eocene times in the Pyrenees, with the development of the Sub-Pyrenean Belt in the north during inactivity of the southern pro-wedge (figs. 14 and 16C).

SUMMARY AND CONCLUSIONS

1. The growth of the Pyrenees was highly asymmetric and evolved through four phases that can be summarized in terms of the generic behavior of the system as follows: A) Early inversion of passive margin extensional faults, initiating the pro-wedge. B) Growth by a combination of frontal accretion and underplating to the pro-wedge; symmetrical and steady record of erosion and foreland basin sedimentation. C) Quiescence of pro-wedge growth, and accretion to retro-wedge. D) Accelerated growth of pro-wedge antiformal stack induced by underplating; accelerated erosion over antiformal stack and increase in sediment discharge to pro-foreland basin; stabilization of outer pro-wedge by sediment blanketing.
2. The distribution of thermochronometric ages across the orogen reveals greatest depths of exhumation (Pyrenean age ZFT ages) in the core of the Axial Zone, with the youngest AFT ages offset into the pro-wedge. The ZFT ages of approximately 50 Ma were generated during maximum rates of frontal accretion to the pro-wedge, and hence maximum retro-ward advection of rock particles within the orogen. The youngest AFT ages of 35 to 20 Ma record the growth of the antiformal stack characterized by underplating, and hence more

vertical trajectories to the surface. This transition from dominantly frontal accretion to underplating is interpreted in terms of stable sliding of the outer fold and thrust belt induced by thick sediment accumulation in ponded piggy-back basins on top of the outer pro-wedge.

3. Discrete element model experiments aid insight into what components of the asymmetry of Pyrenean orogenesis are the predictable outcomes of the asymmetry of subduction, versus those that require additional forcing, whether climatic or tectonic. The models demonstrate the tendency for a strong coupling between erosion and structural deformation in the pro-wedge. This asymmetry is induced by the progressive reduction in rock particle velocities from the pro-wedge accretion front to the retro-wedge and represents the first-order control. Additionally, the model predicts an offset in the maxima of exhumation depth towards the retro-wedge, and a maxima in erosion over the pro-wedge. The model doesn't differentiate frontal accretion versus underplating as a mechanism for accretionary growth of the pro-wedge. The stabilization of the outer pro-wedge, with continued underplating and growth of the inner pro-wedge is a response to localized sediment ponding and erosion respectively, and does not require climatic asymmetry or laterally heterogeneous strength profiles in the underthrust plate (Beaumont and others, 2000).

ACKNOWLEDGMENTS

This project has evolved through many discussions with colleagues, particularly with Sean Willett on the mechanics of thrust wedges and orogenesis. Andrew Meigs and Jaume Vergés are thanked for numerous discussions on the Pyrenees. Feedback on the manuscript from Peter van der Beek and Geoff Batt helped clarify and correct aspects. Journal reviewers Josep Anton Muñoz, Claudia Lewis and Sean Willett are thanked for their comments. Funding has been through the Carnegie Institute, University of Birmingham, NERC studentships to Gibson and Naylor and a Scottish Higher Education Funding Council RDG grant (CRUST).

References

Allen, P. A., and Mange-Rajetzky, M., 1982, Sediment dispersal and palaeohydraulics of Oligocene rivers in the eastern Ebro Basin: Sedimentology, v. 29, p. 705–716.

Anadón, P., and Roca, E., 1996, Geological setting of basins in NE Spain, *in* Friend P. F., and Dabrio, C. J., editors, Tertiary basins of Spain, the stratigraphic record of crustal kinematics: Cambridge, England, Cambridge University Press, p. 43–48.

BRGM (Bureau de Recherches Géologiques et Minières), 1973, Carte Géologique de la France à 1/50,000, Le Mas D'Azil, XX–46.

Batt, G. E., 2001, The approach to steady-state thermochronological distribution following orogenic development in the Southern Alps of New Zealand: American Journal of Science, v. 301, p. 374–384.

Batt, G. E., and Brandon, M. T., 2002, Lateral thinking: 2-D interpretation of thermochronology in convergent orogenic settings: Tectonophysics, v. 349, p. 185–201.

Batt, G. E., and Braun, J., 1997, On the thermo-mechanical evolution of compressional orogens: Geophysical Journal International, v. 128, p. 364–382.

Batt, G. E., Brandon, M. T., Farley, K. A., and Roden-Tice, M., 2001, Tectonic synthesis of the Olympic Mountains segment of the Cascadia wedge, using two-dimensional thermal and kinematic modeling of thermochronological ages: Journal of Geophysical Research, v. 106, p. 26731–26746.

Beaumont, C., Fullsack, P., and Hamilton, J., 1992, Erosional control of active compressional orogens, *in* McClay, K., editor, Thrust Tectonics: London, Chapman and Hall, p. 1–18.

Beaumont, C., Kamp, P. J. J., Hamilton, J., and Fullsack, P., 1996, The continental collision zone, South Island New Zealand; Comparisons of geodynamic models and observations: Journal of Geophysical Research, v. 101, p. 3333–3359.

Beaumont, C., Kooi, H., and Willett, S., 1999, Coupled tectonic-surface process models with applications to rifted margins and collisional orogens, *in* Summerfield, M. A., editor, Geomorphology and Global Tectonics: New York, Wiley, p. 29–55.

Beaumont, C., Muñoz, J. A., Hamilton, J., and Fullsack, P., 2000, Factors controlling the Alpine evolution of the central Pyrenees inferred from a comparison of observations and geodynamical models: Journal of Geophysical Research, v. 105, p. 8121–8145.

Beamud, E., Garcés, M., Cabrera, L., Muñoz, J. A., and Almar, Y., 2003, A new middle to late Eocene continental chronostratigraphy from NE Spain: Earth and Planetary Science Letters, v. 216, p. 501–514.

Berger, J. P., 1992, Correlative chart of the European Oligocene and Miocene: Application to the Swiss Molasse Basin: Eclogae Geolicae Helvetiae, v. 85, p. 573–609.

Bernet, M., Brandon, M., Garver, J., Reiners, P., and Fitzgerald, P. G., 2002, Determining the Zircon fission track closure temperature: Geological Society of America Cordilleran Section 98th Annual Meeting published abstracts.

Bond, R. M. G., and McClay, K., 1995, Inversion of a Lower Cretaceous extensional basin, south central Pyrenees, Spain, *in* Buchanan, J. G., and Buchanan, P. G., editors, Basin Inversion: Geological Society of London Special Publication, v. 88, p. 415–431.

Bourrouilh, R., Richert, J. P., and Zolnai, G., 1995, The North Pyrenean Aquitaine Basin, France: Evolution and hydrocarbons: Bulletin of the American Association of Petroleum Geologists, v. 79, p. 831–853.

Brandon, M., Roden-Tice, M. K., and Garver, J. I., 1998, Late Cenozoic exhumation of the Cascadia accretionary wedge in the Olympic mountains, NW Washington State: Geological Society of America Bulletin, v. 110, p. 985–1009.

Braun, J., 2002, Quantifying the effect of recent relief changes on age-elevation relationships: Earth and Planetary Science Letters, v. 200, p. 331–343.

——— 2003, Pecube: a new finite-element code to solve the 3D heat transport equation including the effects of a time-varying, finite amplitude surface topography: Computers and Geosciences, v. 29, p. 787–794.

Brunet, M. F., 1986, The influence of the evolution of the Pyrenees on adjacent basins: Tectonophysics, v. 129, p. 343–354.

Burbank, D. W., Raynolds, R. G., and Johnson, G. D., 1986, Late Cenozoic tectonics and sedimentation in the north-western Himalayan foredeep: II. Eastern limb of the Northwest Syntaxis and regional synthesis *in* Allen, P. A., and Homewood, P., editors, Foreland Basins: Special Publication of the International Association of Sedimentologists, v. 8, p. 293–306.

Burbank, D. W., Puigdefàbregas, C., and Muñoz, J. A., 1992. The chronology of the Eocene tectonic and stratigraphic development of the Eastern Pyrenean foreland basin, North East Spain: Bulletin of the Geological Society of America, v. 104, p. 1101–1120.

Burbank, D. W., Blythe, A. E., Putkonen, J., Pratt-Sitaula, B., Gabet, E., Oskin, M., Barros, A., and Ojha, T. P., 2003, Decoupling of erosion and precipitation in the Himalayas: Nature, v. 426, p. 652 – 655.

Burbidge, D. R., and Braun, J., 2002, Numerical models of the evolution of accretionary wedges and fold and thrust belts using the distinct-element method: Geophysical Journal Intrenational, v. 148, p. 542–561.

Cederbom, C., Sinclair, H. D., Schlunnegger, F., and Rahn, M. K., 2004, Climate-induced rebound and exhumation of the European Alps: Geology, v. 32, p. 709–712.

Choukroune, P., and ECORS Team, 1989 The ECORS Pyrenean deep seismic profile reflection data and the overall structure of an orogenic belt: Tectonics, v. 8, p. 23–39.

Coney, P. J., Muñoz, J. A., McClay, K. R., and Evenchick, C. A., 1996, Syntectonic Burial and Post-Tectonic Exhumation of The Southern Pyrenees Foreland Fold-Thrust Belt: Journal of the Geological Society of London, v. 153, p. 9–16.

Cundall, P. A., and Strack, O. D. L., 1979, A discrete numerical model for granular assemblies: Géotechnique, v. 29, p. 47–65.

DeCelles, P. G., 1984, Late Cretaceous-Paleocene synorogenic sedimentation and kinematic history of the Sevier thrust belt, northeast Utah and southwest Wyoming: Geological Society of America, Bulletin, v. 106, p. 32–56.

Deffontaines, B., Lee, J. C., Angelier, J., Carvalho, J., and Rudant, J. P., 1994, New geomorphic data in the active Taiwan orogen: A multisource approach: Journal of Geophysical Research, v. 99, B10, p. 20243–20266.

Deramond, J., Souquet, P., Wallez, M. J. F., and Specht, M., 1993, Relationships between thrust tectonics and sequence stratigraphy by surfaces in foredeeps: models and examples from the Pyrenees, *in* Williams, G. D., and Dobb, A., editors, Tectonics and Seismic Sequence Stratigraphy: Geological Society of London, Geological Society Special Publication, v. 71, p. 193–219.

Desegaulx, P., Roure, F., and Villein, A., 1990, Structural evolution of the Pyrenees: tectonic inheritance and flexural behavior of the continental crust: Tectonophysics, v. 182, p. 211–255.

Donelick, R. A., and Miller, D. S., 1991, Enhanced TINT fission track densities in low spontaneous track density apatites using 252Cf-derived fission fragment tracks: A model and experimental observations: Nuclear Tracks and Radiation Measurements, v. 18, p. 301–307.

Fischer, M. W., 1984, Thrust tectonics in the northern Pyrenees: Journal of Structural Geology, v. 6, p. 721–726.

Fitzgerald, P. G., Muñoz, J. A., Coney, P. J., and Baldwin, S. L., 1999, Asymmetric exhumation across the Pyrenean orogen: implications for the tectonic evolution of a collisional orogen: Earth and Planetary Science Letters, v. 173, p. 157–170.

Garwin, L., ms, 1985, Fission track dating and tectonics in the eastern Pyrenees: United Kingdom, Cambridge University, Ph.D. thesis, 320 p.

Hallet, B., Hunter, L., and Bogen, J., 1996, Rates of erosion and sediment evacuation by glaciers: a review of field data and their implications: Global and Planetary Change, v. 12, p. 213–235.

Homewood, P., Allen, P. A., and Williams, G. D., 1986, Dynamics of the Molasse Basin in western Switzerland, *in* Allen, P. A., and Homewood, P., editors, Foreland Basins: Oxford, Blackwell Science, International Association of Sedimentologists Special Publication, v. 8, p. 119–217.

Jordan, T. E., 1981, Thrust loads and foreland basin evolution, Cretaceous, western United States: American Association of Petroleum Geologists Bulletin, v. 65, p. 2506–2520.
Kamp, P. J. J., and Tippett, J. M., 1993, Dynamics of Pacific Plate crust in the South Island (New Zealand) zone of oblique continent- continent convergence: Journal of Geophysical Research, v. 98, p. 16105–16118.
Ketcham, R. A., Donelick, R. A., and Donelick, M. B., 2000, AFTSolve: A program for multi-kinetic modeling of apatite fission-track data: Geological Materials Research, v. 2, n. 1.
Koons, P., 1990, Two-sided orogen: collision and erosion from the sand-box to the Southern Alps: Geology, v. 18, p. 679–682.
——— 1995, Modeling the topographic evolution of collisional mountain belts: Annual Review of Earth and Planetary Sciences, v. 23, p. 375–408.
Lamb, A., and Davis, P., 2003, Cenozoic climate change as a possible cause for the rise of the Andes: Nature, v. 425, p. 792–796.
Lanaja, J. M., Querol, R., and Navarro, A., 1987, Contribucion de la exploracion petrolifera al Conocimiento de la geologia d'Espana: Madrid, Spain, I. G. M. E. 1, v. 17, 465 p.
Meigs, A., 1997, Sequential development of selected Pyrenean thrust faults: Journal of Structural Geology, v. 19, p. 481–502.
Meigs, A., and Burbank, D. W., 1997, Growth of the South Pyrenean orogenic wedge: Tectonics, v. 16, p. 239–258.
Meigs, A., Vergés, J., and Burbank, D. W., 1996, Ten-million-year history of a thrust sheet: Geological Society of America Bulletin, v. 108, p. 1608–1625.
Mellere, D., 1993, Thrust-generated, back-fill stacking of alluvial fan sequences, south-central Pyrenees, Spain (La Pobla de Segur Conglomerates), *in* Frostick, L. E., and Steel, R. J., editors, Tectonic Controls and Signatures in Sedimentary Successions: Special Publication of the International Association of Sedimentologists, v. 20, p. 259–276.
Montgomery, D. R., Balco, G., and Willett, S. D., 2002, Climate, tectonics, and the morphology of the Andes: Geology, v. 29, p. 579–582.
Morris, R. G., Sinclair, H. D., and Yelland, A. J., 1998, Exhumation of the Pyrenean orogen: implications for sediment discharge: Basin Research, v. 10, p. 69–85.
Muñoz, J. A., 1992, Evolution of a continental collision belt: ECORS-Pyrenees crustal balanced cross-section, *in* McClay, K., Thrust Tectonics: London, Chapman and Hall, p. 235–246.
Muñoz, J. A., Martinez, A., and Vergés, J., 1986, Thrust sequences in the Spanish Pyrenees: Journal of Structural Geology, v. 8, p. 399–405.
Muñoz-Jiménez, A., and Casas-Sainz, A. M., 1997, The Rioja Trough (N Spain): tectonosedimentary evolution of a symmetric foreland basin: Basin Research, v. 9, p. 65–85.
Mutti, E., and Sgavetti, M., 1987, Sequence stratigraphy of the Upper Cretaceous Aren strata in the Orcau-Aren region, south-central Pyrenees, Spain: distinction between eustatically and tectonically controlled depositional sequences: Annali dell'Università di Ferrara, v. 1, p. 1–22.
Mutti, E., Remacha, E., Sgavetti, M., Rosell, J., Valloni, R., and Zamorano, M., 1985, Stratigraphy and facies characteristics of the Eocene Hecho Group turbidite systems, South-central Pyrenees, *in* Mila, M. D., and Rosell, J., editors, Excursion Guidebook of the 6th European Regional Meeting: Lerida, Spain, International Association of Sedimentologists, p. 521–576.
Mutti, E., Séguret, M., and Sgavetti, M., 1988, Sedimentation and deformation in the Tertiary sequences of the Southern Pyrenees, Field Guidebook No. 7: American Association of Petroleum Geologists Mediterranean Basins Conference, p. 169.
Naylor, M., Sinclair, H. D., Willett, S., and Cowie, P., 2005, A discrete element model for orogenesis and accretionary wedge growth: Journal of Geophysical Research, v. 110.
Norris, R. J., Koons, P. O., and Cooper, A. F., 1990, The oblique convergent plate boundary in the South Island of New Zealand: implications for ancient collisional zones: Journal of Structural Geology, v. 12, p. 715–725.
Oriel, S. S., and Armstrong, F. C., 1966, Times of thrusting in Idaho-Wyoming thrust belts: reply: American Association of Petroleum Geologists Bulletin, v. 50, p. 2614–2621.
Pazzaglia, F. J., and Brandon, M. T., 2001, A fluvial record of long-term, steady-state uplift and erosion across the Cascadia forearc high, western Washington State: American Journal of Science, v. 301, p. 385–431.
Pérez-Rivarés, F. J., Garcés, M., Arenas, C., and Pardo, G., 2002, Magnetocronologia de la sucesion Miocena de la Sierra De Alcubierre (Sector Central de la Cuence del Ebro): Revista Sociedad Géologica de España, v. 15, p. 210–225.
Pfiffner, O. A., Ellis, S., and Beaumont, C., 2000, Collision tectonics in the Swiss Alps: insight from geodynamic modeling: Tectonics, v. 19, p. 1065–1094.
Pinter, N., and Brandon, M. T., 1997, How erosion builds mountains: Scientific American, v. 276, p. 60–65.
Pous, J., Muñoz, J. A., Ledo, J. J., and Liesa, M., 1995, Partial melting of subducted continental lower crust in the Pyrenees: Geological Society of London, Journal of the Geological Society, v. 152, p. 217–220.
Puigdefàbregas, C., and Souquet, P., 1986, Tectono-sedimentary cycles and depositional sequences of the Mesozoic and Tertiary from the Pyrenees, *in* Banda E., and Wickham, S. M., editors, The Geological Evolution of the Pyrenees: Tectonophysics, v. 129. p. 173–203.
Puigdefàbregas, C., Muñoz, J. A., and Marzo, M., 1986, Thrust belt development in the eastern Pyrenees and related depositional sequences in the southern foreland basin, *in* Allen, P. A., and Homewood, P., editors, Foreland Basins: Special Publication of the International Association of Sedimentologists, v. 8, p. 229–246.
Puigdefàbregas, C., Muñoz, J. A., and Vergés, J., 1992, Thrusting and foreland basin evolution in the Southern Pyrenees, *in* McClay, K., editor, Thrust Tectonics: London, Chapman and Hall, p. 247–254.

Reiners, P. W., Zuyi, Z., Ehlers, T. A., Changhai, Xu., Brandon, M. T., Donelick, R. A., and Nicolescu, S., 2003, Post-orogenic evolution of the Dabie Shan, Eastern China, from (U-Th)/He and fission-track thermochronology: American Journal of Science, v. 303, p. 489–518.

Riba, O., Reguant, S., and Villena, J., 1983, Ensayo de syntesis estratigráfica y eolutiva de la cuenca terciaria del Ebro, *in* Libro Jubilar J. M. Rios, Geologia de Espana: Madrid, Instituto Geologico y Minero de Espana, v. II, p. 131–159.

Roe, G. H., Montgomery, D. R., and Hallet, B., 2003, orographic precipitation and the relief of mountain ranges: Journal of Geophysical Research, v. 108 (B6) 2315, doi:10.1029/2001JB001521.

Roest, W. R., and Srivastava, S. P., 1991, Kinematics of the plate boundaries between Eurasia, Iberia and Africa in the North Atlantic from the late Cretaceous to the present: Geology, v. 19, p. 613–616.

Schedl, A., and Wiltschko, D. V., 1984, Sedimentological effects of a moving terrain: Journal of Geology, v. 92, p. 273–287.

Schlunegger, F., and Willett, S., 1999, Spatial and temporal variations in exhumation of the central Swiss Alps and implications for denudation mechanisms, *in* Ring, U., Brandon, M. T., Lister, G. S., and Willett, S. D., editors, Exhumation Processes: Normal Faulting, Ductile Flow and Erosion: Geological Society of London, Geological Society Special Publication, v. 154, p. 1576–179.

Séguret, M., ms, 1972, Etude tectonique des nappes et séries décolées de la partie centrale du versant sud des Pyrénées: Montpelier, Ph.D. thesis, Publications USTELA, Série Géeologique Structuralle, No. 2.

Sinclair, H. D., and Allen, P. A., 1992, Vertical versus horizontal motions in the Alpine orogenic wedge: stratigraphic response in the foreland basin: Basin Research, v. 4, p. 215–233.

Specht, M., Deramond, J., and Souquet, P., 1991, Relationships between tectonics and sedimentation in foredeeps: use of stratigraphic isochron surfaces as markers of the deformation: Bulletin Societé Géologique Française, v. 162, p. 553–562.

Storti, F., and McClay, K., 1995, Influence of syntectonic sedimentation on thrust wedges in analogue models: Geology, v. 23, p. 999–1002.

Stüwe, K., and Hintermüller, M., 2000, Topography and isotherms revisited: the influence of laterally migrating drainage divides: Earth and Planetary Science Letters, v. 184, p. 287–303.

Stüwe, K., White, L., and Brown, R., 1994, The influence of eroding topography on steady state isotherms: Application to fission track analysis: Earth and Planetary Science Letters, v. 124, p. 63–74.

Suppe, J., 1981, Mechanics of mountain building and metamorphism in Taiwan: Memoirs of the Geological Society of China, v. 4, p. 67–90.

Teixell, A., 1998, Crustal structure and orogenic material budget in the west central Pyrenees: Tectonics, v. 17, p. 395–406.

Vergés, J., 1999, Estudi geologic del vessant sud del Pirineu oriental I central. Evolucio cinematica en 3D. Col-leccio Monografies tècniques, num. 7: Barcelona, Institut Cartografic de Catalunya, 194 p.

Vergés, J., and Muñoz, J. A., 1990, Thrust sequences in the southern central Pyrenees: Bulletin Societé Géologique Française, v. 8, p. 265–271.

Vergés, J., Millàn, H., Roca, E., Muñoz, J. A., Marzo, M., Cirés, J., Den Bezemer, T., Zoetemeijer, R., and Cloetingh, S., 1995, Eastern Pyrenees and related foreland basins: pre-, syn- and post-collisional crustal scale cross-sections: Marine and Petroleum Geology, v. 12, p. 893–915.

Vergés, J., Marzo, M., Santaeularia, T., Serra-Kiel, J., Burbank, D. W., Muñoz, J. A., and Gimenez-Montsant, J., 1998, Quantified vertical motions and tectonic evolution of the SE Pyrenean foreland basin, *in* Mascle, A., Puigdefàbregas, C., Luterbacher, H. P., and Fernandez, M., editors, Cenozoic Foreland Basins of Western Europe: Geological Society of London, Geological Society Special Publication, v. 134, p. 107–134.

Vergés, J., Fernàndez, M., and Martinez, A., 2002, The Pyrenean orogen: pre-syn- and post-collisional evolution, *in* Rosenbaum, G., and Lister, G. S., editors, Reconstruction of the evolution of the Alpine Himalayan Orogen: Journal of the Virtual Explorer, v. 8, p. 57–76.

Villena, J., Pardo, G., Pérez, A., Muñoz, A., and González, A., 1996, The Tertiary of the Iberian margin of the Ebro Basin: palaeogeography and tectonic control, *in* Friend, P. F., and Dabrio, C. J., editors, Tertiary Basins of Spain: the Stratigraphic Record of Crustal Kinematics: World and Regional Geology, v. 6: Cambridge, Cambridge University Press, p. 83–88.

Wayne, D. M., and McCaig, A. M., 1998, Dating fluid flow in shear zones: Rb-Sr and U-Pb studies of syntectonic veins in the Neouvielle Massif, Pyrenees, *in* Parnell, J., editor, Dating and Duration of Fluid Flow and Fluid Rock Interaction: Geological Society of London, Geological Society Special Publication, v. 144, p. 129–135.

Willett, S. D., 1992, Dynamic and kinematic growth and change of a coulomb wedge, *in* McClay, K., editor, Thrust Tectonics: New York, Chapman and Hall, p. 19–31.

——— 1999, Orogeny and orography: The effects of erosion on the structure of mountain belts: Journal of Geophysical Research, v. 104, p. 28957–28981.

Willett, S. D., and Brandon, M. T., 2002, On steady state in mountain belts: Geology, v. 30, p. 175–178.

Willett, S. D., Beaumont, C., and Fullsack, P., 1993, Mechanical models for the tectonics of doubly vergent compressional orogens: Geology, v. 21, p. 371–374.

Willett, S. D., Slingerland, R., and Hovius, N., 2001, Uplift, shortening, and steady-state topography in active mountain belts: American Journal of Science, v. 301, p. 455–485.

Williams, E. A., Ford, M., Vergés, J., and Artoni, A., 1998, Alluvial gravel sedimentation in a contractional growth fold setting, Sant Lorenc de Morunys, southeastern Pyrenees, *in* Mascle, A., Puigdefàbregas, C., Luterbacher, H. P., and Fernàndez, M., editors, Cenozoic Foreland Basins of Western Europe: Geological Society of London, Geological Society Special Publication, v. 134, p. 69–106.

Wiltschko, D. V., and Dorr, J. A., Jr., 1983, Timing of deformation in thrust belt and foreland of Idaho, Wyoming and Utah: American Association of Petroleum Geologists, v. 67, p. 1304–1322.

Yelland, A. J., 1990 Fission track thermotectonics in the Pyrenean orogen: Nuclear Tracks and Radiation Measurements, v. 17, p. 3–299.

——— ms, 1991, Thermo-tectonics of the Pyrenees and Provence from fission track studies: London, University of London, Ph.D. thesis.

Zeyen, H., and Fernández, M., 1994, Integrated lithospheric modeling combining thermal, gravity, and local isostasy analysis: application to the NE Spanish Geotransect: Journal of Geophysical Research, v. 99, p. 18089–18102.

Zoetemeijer, R., Deselgaulx, P., Cloetingh, S., Roure, F., and Moretti, I., 1990, Lithospheric dynamics and tectono-stratigraphic evolution of the Ebro Basin: Journal of Geophysical Research, v. 95, p. 2701–2711.